Optical and Photo-Electrochemical Properties of Nanoporous Gold

Combined report of FIT-Internship and Bachelor Thesis

Mart Salverda
Student number: s1916432

Daily supervisor:
dr. E. Detsi

Group Leader:
prof. dr. J.Th.M. de Hosson

Bachelor project in cooperation with Msc. L. de Jeer

Materials Science Group
Zernike Institute for Advanced Materials
University of Groningen

August 22, 2013

Preface

Dear Reader,

A few words on the motivation to present a combined report. It was decided to combine the reports due to a few reasons:

The first reason being that both projects involved nanoporous gold (NPG). The FIT-internship dealt with synthesizing NPG samples and investigating the relation between the transmission spectrum and the microstructure of the NPG. The research for the Bachelor thesis consisted of providing a theoretical background for a photoelectrochemical cell, containing NPG, with the ability to store the energy of sunlight into hydrogen gas.

Secondly, both projects involve the **localized surface plasmon resonance** effect (LSPR). This phenomenon is of importance to understanding the relation between the transmission spectrum and the microstructure, as was investigated during the FIT-internship, and also to understanding the possibilities of NPG converting the energy of (sun)light into electrical and chemical energy, which are explored in the Bachelor research. The theoretical background for this LSPR is the same for both projects, so in the case of a combined report, it only has to be presented once.

Thirdly, 'the Bigger Picture'. The research done during the Bachelor project made that of the FIT-internship more relevant than I could ever have tried to accomplish in the motivational introduction of a separate FIT-internship report. Perhaps to the reader it would not have made much difference if the reports would have been made separately, but for me the connection of both projects is very clear, which also makes both projects even more interesting.

To anyone only interested in the bachelor thesis, for administrative reasons for example: the work that would have been presented in a separate Bachelor Thesis is now divided over two chapters. Chapter 1 contains the background on LSPR, which, as I already explained, is of importance to the research in the Bachelor project. Chapter 3 is basically the main body of what would have been the Bachelor Thesis.

Contents

Chapter 1

Introduction

1.1 Metallic Nanoparticle and Nanoporous Metals

Metallic nanoparticles like the nanorods in figure 1.1 have been found to convert light into electrical or chemical energy (when in combination with a semiconductor)[1]. For future applications, this is very interesting. Think of solar cells. Efficient solar cells are expensive. Alternatives are being researched that are cheaper in production and materials. Also, making existing cell types more efficient would be a desirable result. Plasmonic metals could contribute to achieve both these aims.

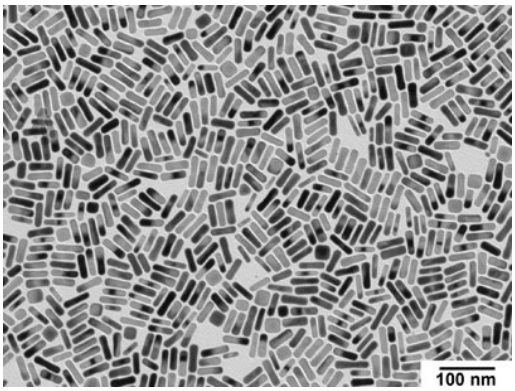

Figure 1.1: Micrograph of nanorods. Image from medtechinsider.com/archives/273.

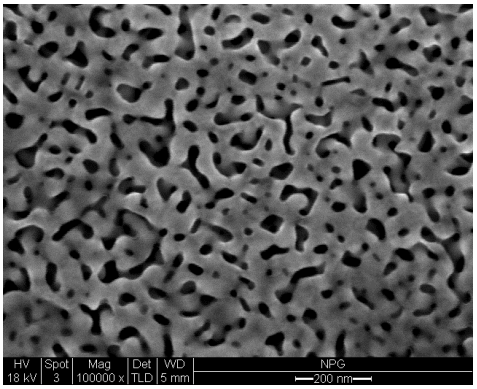

Figure 1.2: Scanning Electron Micrograph of nanoporous gold.

The earth is rich in quite a few metals. It could prove worthwhile to investigate nanostructures of these metals in order to find useful optical properties that allow for efficient conversion of light to other forms of energy. However, not only the kind of metal is important, also the nanostructure and topology. So far, most research in this field has been done on nanoparticles.

Nanoporous metals are metals with a sponge-like structure where the dimensions of the ligaments and pores are in the nanometer range, see figure 1.2 [2]. These nanoporous metals have the benefit that it is a percolating structure, allowing for good conducting properties. If the same light-converting properties of nanoparticles would be present in a nanoporous film, this new class of materials could potentially make solar devices more efficient and/or cheaper .

So far, only a few articles have been published about nanoporous metals. Also the Materials Science group of the University of Groningen is investigating these materials. For example, nanoporous

gold (NPG) has been used by Detsi to fabricate an actuating composite material[2][1].

1.2 Localized Surface Plasmon Resonance

The absorption and transmission of light and the conversion to useful energy by nanoparticles (and possibly nanoporous metals) is due to localized surface plasmon resonance (LSPR). An introduction into this phenomenon is given here.

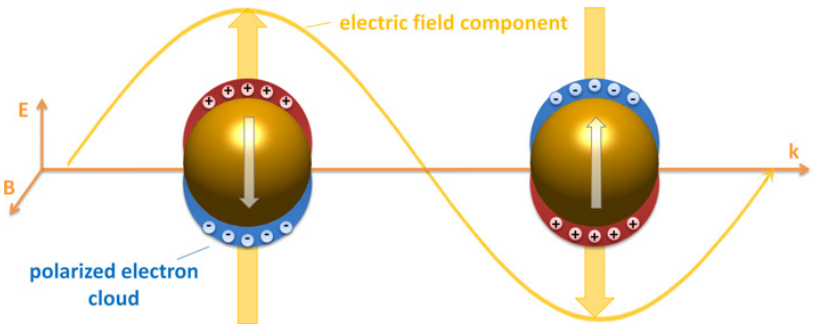

Figure 1.3: Localised Surface Plasmon Resonance [3]. If the metal nanoparticles are smaller than the wavelength of the light, the electron cloud oscillates together with the electric field. At the right light frequency, the electron clouds resonate.

A **plasmon** is a quantization of an oscillation of the free electron gas (or plasma) in a metal [4]. It is a quasi-particle, as, for example, the quantized oscillation in a material is called a phonon. When an electromagnetic wave, like an optical photon, interacts with the surface of a metal, the free electrons in this metal are affected by its electric field. The electron cloud starts to oscillate, resulting in a **surface plasmon**. If the frequency of the optical photons matches the natural frequency of the surface electrons, the surface electron cloud starts to resonate: **surface plasmon resonance**. If the surface has dimensions in the nanometer-regime, the properties of the plasmon are rather different than those of the surface or bulk plasmon. Therefore, this specific plasmon resonance is called **localized surface plasmon resonance** [4].

The frequency of this resonance depends on the material, but also on the shape and dimensions of the nanostructure[5], as will be discussed in section 2.4. A few models exist to calculate the absorption and transmission for certain well-defined nanoparticles (for example, Mie theory is), but they cannot or have not yet been used for nanoporous structures.

1.3 Enhancements by Plasmonic Nanoparticles

Metal nanoparticles have been found to enhance the efficiency of semiconductor light-harvesting devices when in contact or close vicinity. A few different mechanisms are responsible for these enhancements.

In the first place, the absorption of photons by a semiconductor is influenced by an electric field. The rate of electron-hole pair formation due to photon absorption is proportional to the intensity of the local electric field ($\propto |E|^2$)[6][7]. Plasmons are accompanied by a very strong local electric field, up to 10^3 times stronger than the electric field of the light, see figure 1.4. Therefore, around a plasmonic metal nanoparticle that is being illuminated, the illuminated semiconductor becomes more efficient, see figure 1.5.

[1]See this reference for a number of publications of performed by members of the Meterials Science group

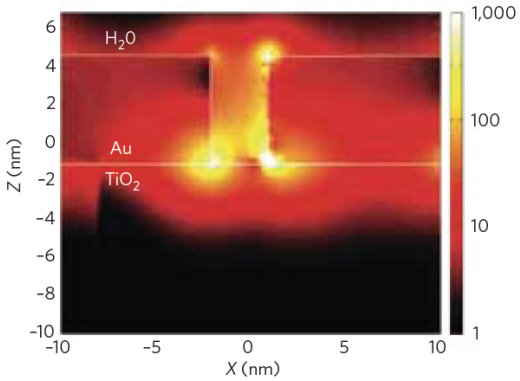

Figure 1.4: Simulation of field enhanced electron-hole production at a water-gold-TiO interface. The colour bar shows the electric field intensity, normalized by the light source intensity: $|E|^2/|E|_0^2$ [6].

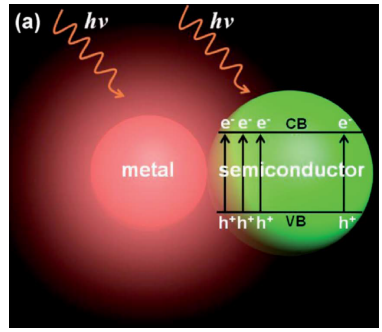

Figure 1.5: Plasmon-enhanced electron-hole pair formation. The glow of the particle represents the electric field in which the rate of pair formation is increased [7].

Also, nanoparticles scatter light (plasmons can decay as photons), which increases the path length of the photons in a volume of semiconductor material, making it more likely to be absorbed, see figure 1.6.

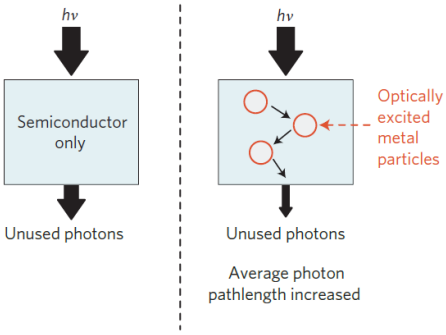

Figure 1.6: Plasmonic nanoparticles increase photon path length in semiconductor material due to scattering and absorption/emission (see figure 1.8) [6].

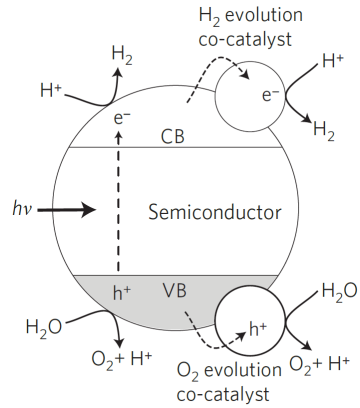

Figure 1.7: Semiconductor water splitting particle with increased efficiency by nanocatalysts [6].

Nanoparticles can also act as a catalyst. The plasmonic properties are not necessarily required for this. As will be explained in section **??**, some materials pass electrons to a redox couple better than others. Hydrogen evolution is a fast reaction on some metals, while it is not on most semiconductors. Therefore, adding catalytic nanoparticles to a semiconductor device that splits water would increase its efficiency, for example. See figure 1.7 for a such a case.

However, the plasmonic nanoparticles can do more. Plasmons do not live forever, but decay via a radiative or non-radiative process, see figure 1.8. The radiative process means a photon is emitted.

This is part of the scattering enhancement discussed earlier (see figure 1.6). The non-radiative decay consists of an electron being excited into a so-called **hot electron**. It is called hot due to the high energy it has compared to the other electrons in the metal.

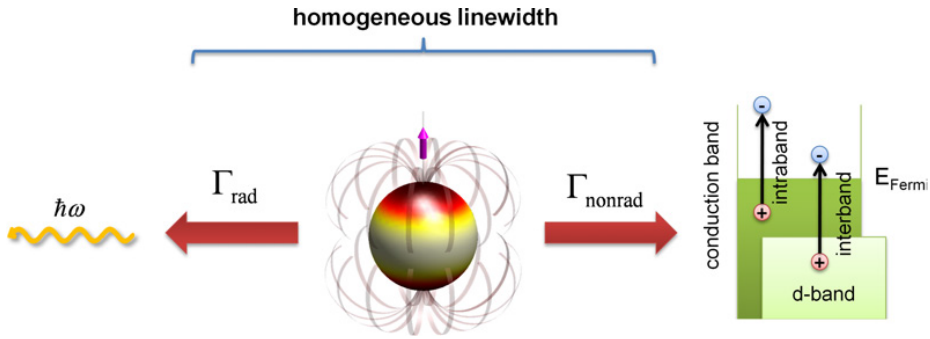

Figure 1.8: The two ways a plasmon can decay: radiative (emission of photon) and non-radiative (excitation of electron-hole pairs) [3].

Figure 1.9: The life times of the different steps, from plasmon to phonon [3].

Localised surface plasmons generally do not live long and have a lifetime of only a few femtoseconds, see figure 1.9. The energy is lost to the surrounding electrons and crystal lattice [8]. In surface plasmons this is even worse, as the oscillation is not confined [8]. The some holds for hot electrons: in nanoparticles they can live up to a few picoseconds, but a bulk metal, they only have a life time in the range or tens of femtoseconds [9]. Also, the more energy a hot electron has, the shorter the lifetime [9].

A hot electron can do things his 'cold brothers' cannot. For example, a hot electron with enough energy can jump across the Schottky barrier of a metal-semiconductor interface, see figure 1.10. If combined with a water splitting semiconductor like the one in figure 1.7, the hot electrons assist in the hydrogen production, see figure 1.12.

Also, if an electron is excited from a lower band, it can leave a **hot hole** which can also have similar interactions with the bands of a semiconductor, see figure 1.11.

Apart from injecting electrons and holes into a semiconductor that facilitates a chemical reaction, they can also drive a chemical reaction themselves. Hot electrons and holes can directly influence a reaction, see figure 1.13.

1.4 Outline of the Report

The underlying -perhaps retrospective- goal of both the FIT-internship and the Bachelor project was to see whether the properties of plasmonic nanoparticles also hold for nanoporous metals. For plasmonic nanoparticles there are many examples of publications in which the particles act as described in the previous sections. However, the different nature of the nanoporous gold could also mean the plasmons and hot electrons and holes in the NPG behave differently, as they are not confined to a small nanoparticle.

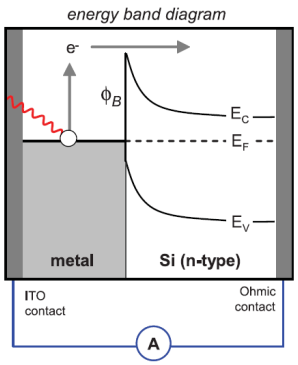

Figure 1.10: Hot electrons cross the Schottky barrier of a metal-Si contact [10][11].

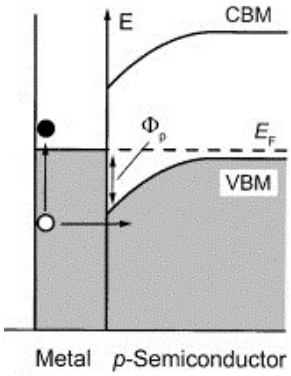

Figure 1.11: A hot hole enters the valence band of a semiconductor[12]

1.4.1 FIT-Internship

Ch. 2 will describe the experiments that were performed and results that were obtained during the FIT-Internship. The goal of this project was to find the connection between the transmission spectrum of a nanoporous gold film and the sizes of pores and ligaments in the nanostructure.

First the sample synthesis is discussed, after which the measurement results are analysed, followed by a theoretical model to compare theory with the measurement results.

1.4.2 Bachelor Project

Ch. 3 will describe some of the work done during the Bachelor project. During this project, the goal was to provide Detsi and De Jeer with theoretical background for their experiments and a theoretical explanation of their results in their Postdoctoral Project and Master Thesis, respectively.

The intention of this project was to create a device that would convert solar energy into chemical energy in the form of hydrogen. One such a device is investigated in detail in this chapter. The initial view of the working mechanism is given, after which an experiment is performed to split water into hydrogen and oxygen. The results of this experiment ask for a revision of the working mechanism. Then, a new mechanism is proposed.

Since both projects (the FIT-internship and the Bachelor project) deal with localized surface plasmons, this chapter (Ch. 1) briefly described the phenomena of plasmons and localized surface plasmon resonance and how metal nanoparticles can enhance or drive chemical reactions, before delving more deeply into the project-specific aspects of structure-dependent resonance (Ch. 2) and the creation of hot electrons (Ch. 3).

References

[1] J. Lee, S. Mubeen, X. Ji, et al. “Plasmonic Photoanodes for Solar Water Splitting with Visible Light”. In: *Nano Lett.* (2012).

[2] E. Detsi. “Metallic Muscles: Enhanced Strain and Electrolyte-Free Actuation”. PhD thesis. University of Groningen: Zernike Institute for Advanced Materials, 2012.

[3] A. Trügler. “Optical Properties Of Metallic Nanoparticles”. PhD thesis. University of Graz, 2011.

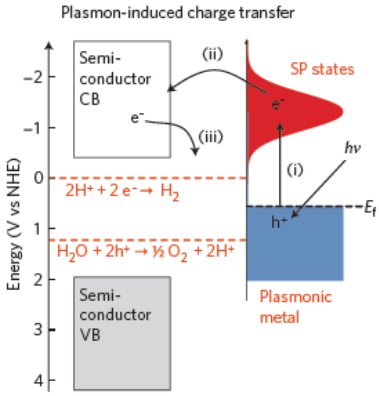

Figure 1.12: Plasmon induced charge transfer. A hot electron enters the conduction band of a semiconductor which splits water [6].

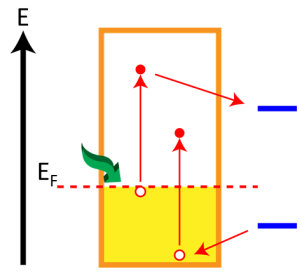

Figure 1.13: Representation of hot electrons and hot holes driving a cathodic and anodic reaction respectively.

[4] K.A. Willets and R.P. Van Duyne. "Localized Surface Plasmon Resonance Spectroscopy and Sensing". In: *Annu. Rev. Phys Chem.* (2007).

[5] X. Xu and M.B. Cortie. "Shape Change and Color Gamut in Gold Nanorods, Dumbbells, and Dog Bones". In: *Advanced Functional Materials* (2006).

[6] S. Linic, P Christopher, and D.B. Ingram. "Plasmonic-metal nanostructures for efficient conversion of solar to chemical energy". In: *Nature Materials* (2011).

[7] M. Xiao, R. Jiang, F. Wang, et al. "Plasmon-Enhanced Chemical Reactions". In: *Journal of Materials Chemistry A* (2013).

[8] S. Link, C. Burda, and other. "Electron Dynamics in Gold and Gold-Silver Alloy Nanoparticles: The Influence of a Nonequilibruim Electron Distribution and the Size Dependence of the Electron-Phonon Relaxation". In: *Journal of Chemical Physics* (1999).

[9] I. Campillo, J.M. Pitarke, A. Rubio, et al. "Inelastic Lifetimes of Hot Electrons in Real Metals". In: *Phys. Rev. Lett.* (1999).

[10] M.W. Knight et al. "Photodetection with Active Optical Antennas". In: *Science* (2011).

[11] S. Mubeen, G. Hernandez-Sosa, et al. "Plasmonic Photosensitization of a Wide Band Gap Semiconductor: Converting Plasmons to Charge Carriers". In: *Nano Lett.* (2011).

[12] H. Nienhauss. "Electronic Excitations by Chemical Reactions on Metal Surfaces". In: *Surface Science Reports* (2002).

Chapter 2

Optical Properties of Nanoporous Gold (FIT-internship)

2.1 Introduction

It has been found that the resonance frequency of nanoparticles depends, among other things, on the shape and dimensions of the particles [1]. Theoretical models have been invented to calculate the resonance frequency of nanoparticles with certain simple geometrical shapes. With this frequency, the transmission and absorption spectrum can be calculated [1]. However, to come up with such a solution for an irregularly shaped particle, let alone a nanoporous material, is rather difficult. Recently a paper has been published by Lang et al.[2] reporting on their observations of the absorption spectra for nanoporous gold. They tailored the size of the pores in the nanoporous film and noticed a change in the transmission peak[1] it linearly shifted towards lower energies (i.e. into the red) for increasing pore size.

Experimental observations in the Materials Science Group contradict this. For increasing pore sizes, the large transmission peak has been found to indeed shift into the red, but also back to the blue again. This indicates that more variables might be playing a role in the peak position than only the pore size.

The goal of FIT-internship was to perform similar experiments as the ones performed by Lang et al.[2] in order to observe whether the peak would indeed shift back and forth and to determine on which parameters the transmission peak depends.

This chapter will go into detail about the synthesis of nanoporous gold films and about tuning the feature sizes at the nano-scale. The section 3.3.2 will present the measured transmission spectra, the SEM images that were taken and an analysis of this data. After that, in section 2.4 a theoretical model will be presented to calculate the transmission spectra for a similar case of nanorods, of which it will be shown that the predictions it generates are in agreement with the data gathered from the NPG samples.

[1] Lang et al.[2] speak of an extinction peak, but our measurements contradict this. The peaks of which they speak are transmission peaks. Even though one might think resonance usually gives rise to an absorption peak, in the case of plasmonic materials, Extraordinary Optical Transmission allows for the opposite. For more information, read [3]

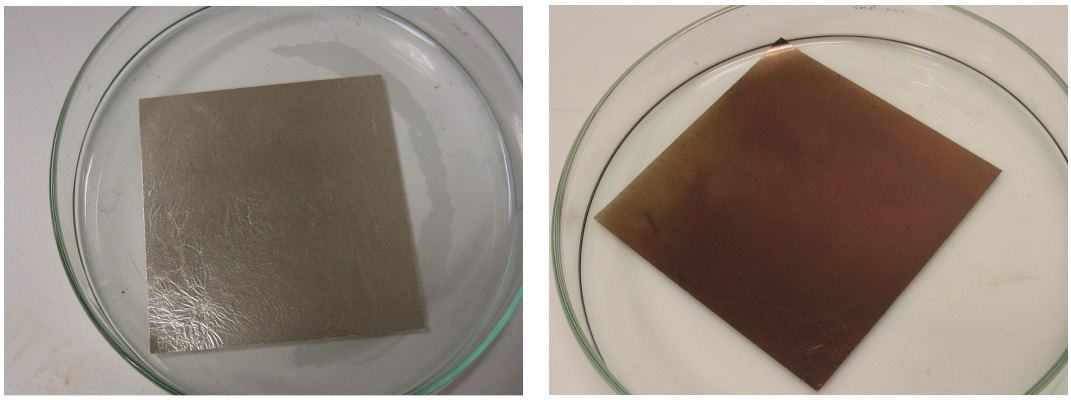

(a) A 100nm-thick white gold leaf before de-alloying (b) The same leaf after de-alloying

Figure 2.1: Dealloying [4]

2.2 Methods and materials

2.2.1 NPG Synthesis

White gold leaves with composition Au35Ag65 (at.%) were chemically de-alloyed in a solution of concentrated nitric acid ($HNO_3(aq) \sim 15M$). During this process, the silver is dissolved into the nitric acid, leaving behind a gold nanoporous structure[2]. The different preparation steps for creating samples of nanoporous gold are found in Appendix A.

Silver has a different LSPR resonance resonance frequency than gold. If some silver remains in the sample, the measured LSPR peak will not be at the resonance wavelength of pure gold, but the peak will be a blend of the resonance peaks of both gold and silver [5]. Since we are mostly interested in the optical properties of gold, we prefer to have as little silver in our samples as possible.

However, the amount of silver in the sample is inversely related to the time the leaf spends de-alloying on the surface of the acidic solution (the longer the sample is kept in acid, the more silver has dissolved). The de-alloying time also has an effect on the the ligament and pore sizes of the nanoporous gold, as is explained in section 2.2.2: the longer the nanoporous gold is kept in acid, the larger the features become [6]. Therefore, it is clear that a trade-off has to be made and one has to find the optimal conditions for the experiments.

It was decided to make sure the amount of silver in the samples is below 5 at. %. This allows for relatively small feature sizes, while the contribution of silver to the resonance peaks is small enough to neglect. In practice, however, the percentage of silver is usually a lot less than this imposed limit.

The composition of a few samples has been checked to see how long a sample has to be kept in acid to meet this requirement. EDX measurements showed that a sample that has been de-alloyed for 10 minutes still consists of $\sim$ 10 at.% of silver, while the sample contains less than 5 at. % after 30 minutes. From now on, only samples that have been in acid for longer than 30 minutes are used in the analysis.

2.2.2 Obtaining the samples and Measurement Data

The white gold leaf was kept in acid. The leaf slowly coarsens (i.e. the features in the nanostructure –pores and ligaments– get bigger) while it is kept there [7]. With intervals of 10 minutes, a small sample was taken from the gold leaf. These sample were rinsed in water to remove most of the dissolved silver and acid from the pores. After rinsing, the sample was placed on a small glass plate

(a microscope slide) and left to dry. This entire procedure was performed three times, to obtain the sample sets 1.1, 1.2 and 1.3.

The first set consisted of samples that had been coarsened for 15 to 185 minutes. By looking at the transmission spectra of these samples (section 2.3.2) it was observed that the peak shifting back and forth happened a few times over time. To prevent the project from becoming too time-consuming, one of these back-and-forth shifts was focused on. See also section 3.7 for recommendations on faster data-analysis. Between 30 and 90 minutes of coarsening such a shift was observed. Therefore, the next two sets (1.2 and 1.3) focus on the same time interval (30-90 minutes).

Note that there are different methods to coarsen NPG. For example, another method is heating gold, granting the gold atoms a higher mobility to reduce their surface energy. Appendix B reports on a few of these methods that have been tried to coarsen the NPG leafs during this project. Why they seemed interesting and why they have not been chosen to be implemented in this project, is explained as well.

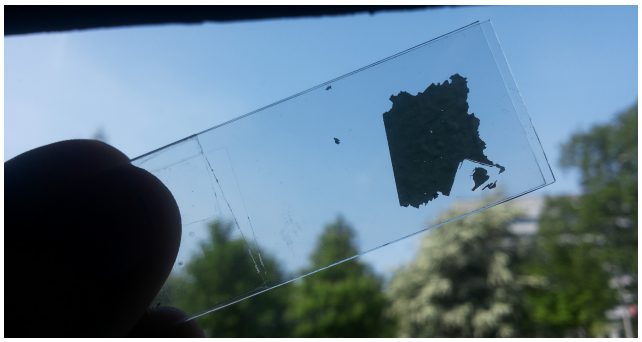

Figure 2.2: The glass plates with a sample of nanoporous gold sandwiched in between.

Figure 2.3: The SEM pin-mount with NPG on 1/4 of a carbon adhesive tab.

Of each sample, a small SEM-sample was taken to be examined in a Scanning Electron Microscope (a Philips XL30S SEM FEG). The small piece of NPG film was obtained by pressing a pin-type SEM mount with 1/4th of a conductive carbon adhesive tab onto the sample. In figure 2.3 such a mount is displayed, with a carbon adhesive tab and a piece of nanoporous gold on top. The images taken with the SEM were examined and the feature sizes were measured in the imaging software Digital Micrograph.

The samples on glass were measured by a standard spectrometer (Perkin-Elmer Lambda 900 UV-Vis-NIR Spectrometer). The spot size was around a few square millimeters. The measurements were performed with water inside the pores of the NPG. In order to do this, another glass plate was placed on top of the sample, sandwiching the sample between two plates. By capillary absorption a few drops of water slowly spread between the glass plates and intro the sample without breaking it. See section 2.3.1 for an explanation of why the measurements were performed with water.

2.2.3 Inhomogeneous process of de-alloying

Unfortunately, it was observed that most of the samples were not homogeneously de-alloyed. Nanoporous gold has a brownish colour and the alloy of gold and silver, also called 'white gold' has, ironically, a silver colour (see figure 2.1). While de-alloying a white gold leaf, the sample slowly turned brown. However, on most of the leaves this did not happen at the same rate across the entire sample. Usually, the edges had become dark while the center had not shown any sign of de-alloying yet.

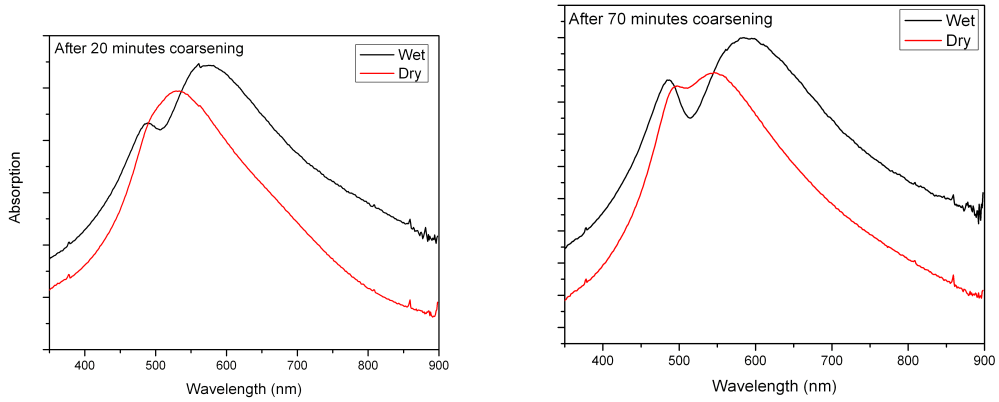

(a) (b)

Figure 2.4: Transmission spectra of samples that have been coarsened in acid for (a) 20 minutes and (b) 70 minutes. The red and black lines represent the measurements with air and water as surrounding medium respectively.

Since the inhomogeneity was more pronounced in a solution with a lower concentration of nitric acid (∼7.5M), all sample sets were synthesised with gold leaves de-alloyed in high concentration (∼15M) nitric acid.

2.3 Results

2.3.1 Effect of the surrounding medium on the spectrum

A preliminary measurement of the transmission spectra was performed, before the three main sets were synthesized. The surrounding medium was air (i.e. the samples were dry). The resulting transmission spectra showed that the two peaks in the spectra of short-coarsened samples overlapped extensively, making it impossible to distinguish the two. For longer coarsening times, the two peaks do separate. For these two spectra, see the red lines in figure 2.4.

As was suggested by the results of Lang et al.[2], the position of the transmission peaks in the spectrum of a nanoporous gold film does not only depend on the characteristics of the nanostructure, but also on the surrounding medium. They claimed that the peaks also shift depending on the refractive index of the medium. We therefore chose to use water as the surrounding medium, since it is an easy material to work with and has a rather different refractive index than air, which was the surrounding medium for the dry sample.

The results of measuring the transmission spectra of the same samples were a lot better when using water as a surrounding medium. The two peaks were better distinguishable for all samples. See the blue lines in figure 2.4 for the new 'wet' transmission spectra, compared with their respective 'dry' measurements. From this moment on, all the measurements were performed using water as the surrounding medium.

2.3.2 Transmission spectra

The transmission spectra of the three sample sets are shown in figure 2.5.

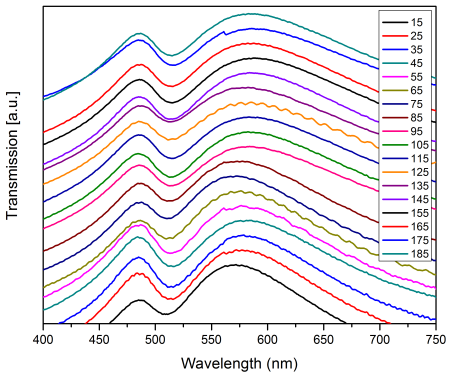

(a) Set 1.1

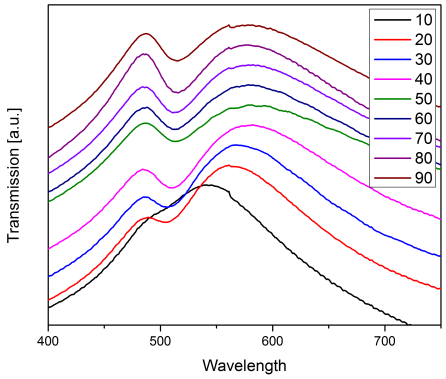

(b) Set 1.2

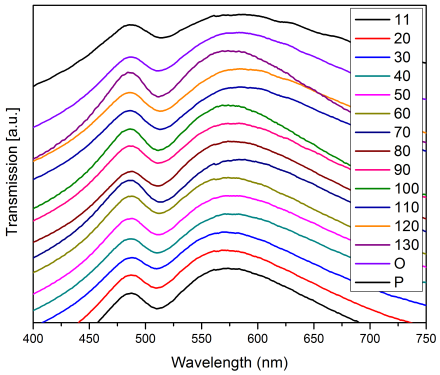

(c) Set 1.3

Figure 2.5: The plots of the transmission spectra for all the samples of the three sets. The spectra are in order of coarsening time, with the shortest time on the bottom. The peak can be seen shifting to the right and to the left. This is especially clear in set 1.2.

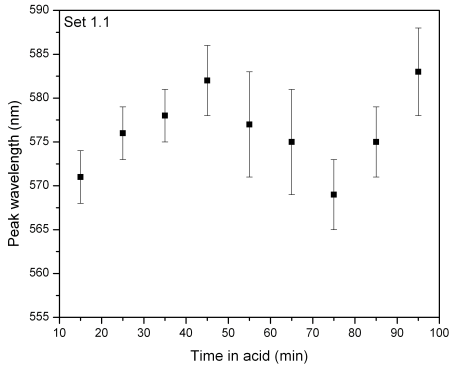

(a) Set 1.1

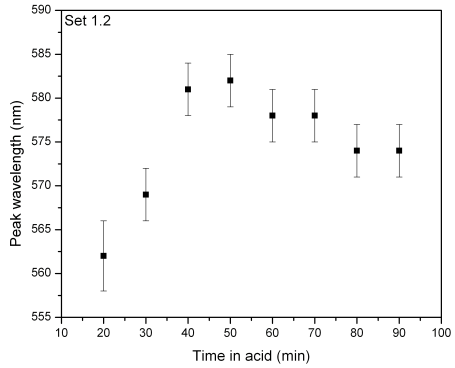

(b) Set 1.2

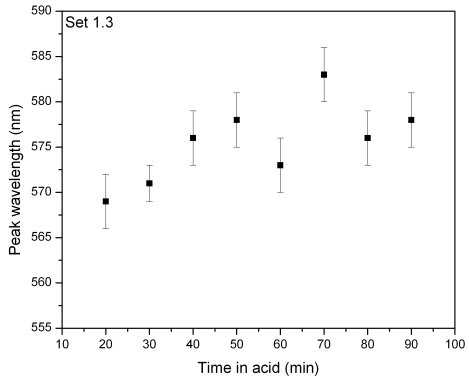

(c) Set 1.3

Figure 2.6: The plots of the transmission peak wavelentgh versus the coarsening time for the three sets. It can clearly be seen that not only the peak wavelength does not increase linearly with coarsening time, but even decreases in some cases.

It can be observed that especially the long-wavelength peak shifts for different coarsening times. However, what also becomes apparent is that this shift is not continuously into the red: it goes back and forth a few times. This behaviour is observed for all three sets. From now on, only the data obtained for samples that have coarsened for a time between 10 and 100 minutes are used in the analysis. This has been done mainly because of the workload, but also because one of the sets did not contain any more data. Over this range, the best comparison can be made between the three sets.

In figure 2.6, the position of the transmission peaks has been plotted versus coarsening time for all three sets.

2.3.3 SEM images

On each SEM-sample 5 pictures were taken at random spots, though all with the same magnification. The ligament size (diameter) and the pore size (diameter) of 10 randomly chosen well defined

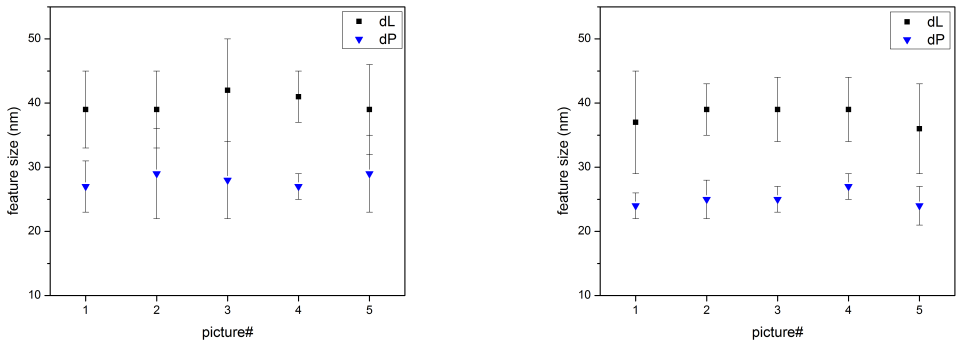

(a) (b)

Figure 2.7: The means and standard deviations of the ligaments and pores, measured on all pictures of two random samples. It can be concluded that the feature sizes are comparable across a sample.

ligaments and pores were measured on each picture. This had to be done manually, since there was no software available that could identify diameters of especially the pores. This is due to the fact that the picture is a projection of a 3D structure. Imaging software uses contrast to determine which parts of the picture belong together. The difficulty with this 3D porous structure is that the software cannot see whether a pore goes into the surface perpendicular or at an angle, since it is not able to use the contrast gradients to see the projection of a 3D structure, while humans can. This is of vital importance for determining the diameter of a pore, so it had to be done by hand.

If a line is drawn on a picture in Digital Micrograph (DM), the software is able to calculate the length of the line on the scale of your picture. This is used to measure lengths in SEM pictures. Apart from this, DM calculates the mean and the standard deviation of all drawn lines. To check for homogeneity, in figure 2.7 the mean and standard deviation of the ligament and pore diameter has been plotted for all pictures on a few random samples.

This way the mean and standard deviation of the ligament diameter and the pore diameter could be easily obtained for every picture and for every sample.

In figure 2.7 it is shown that on a few random samples, the data collected from the 5 pictures agree with each other.

In figures 2.8 the ligament and pore diameter have been plotted for the three main sets of samples versus de-alloying time. It can be seen that pore diameter and ligament diameter do not grow in the same way in all three sets.

2.3.4 Correlation

The next step is combining the transmission measurements with the SEM-data and trying to determine whether there is a correlation between transmission peak wavelength and pore diameter, ligament diameter or a function of these properties.

In figure 2.9 the peak wavelength has been plotted versus ligament diameter. It shows that there is no one-on-one correlation between transmission peak wavelength and ligament diameter.

In figure 2.10 the peak wavelength has been plotted versus pore diameter. Looking at this plot, there is no obvious correlation between these two variables either.

When plotting the peak wavelength versus the ratio of ligament and pore diameter, the size of the errors makes it difficult to draw any conclusions.

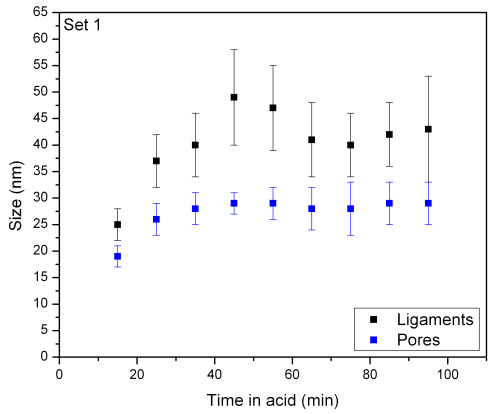

(a) Set 1.1

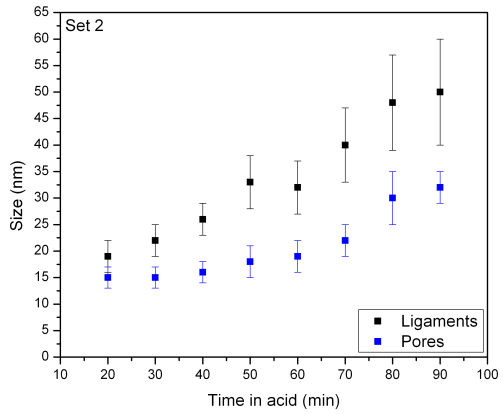

(b) Set 1.2

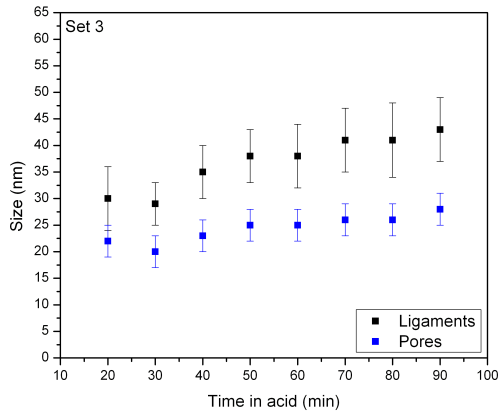

(c) Set 1.3

Figure 2.8: The plots of the transmission peak wavelentgh versus the coarsening time for the three sets. It is clearly observed that the three sets show different coarsening behaviour.

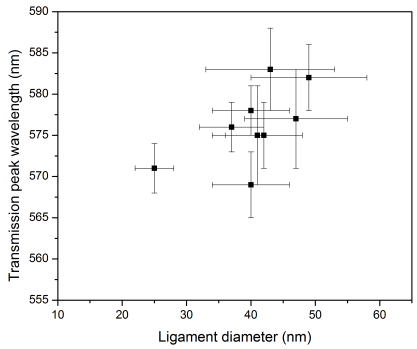

(a) Set 1.1

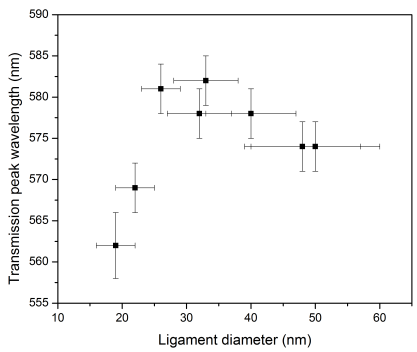

(b) Set 1.2

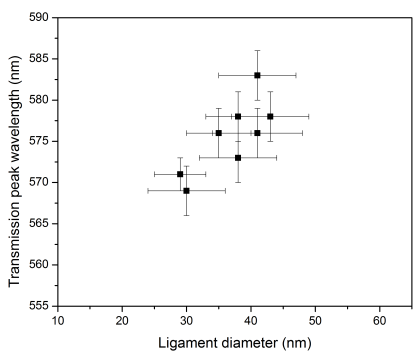

(c) Set 1.3

Figure 2.9: Peak wavelength versus ligament diameter. There is no clear correlation between these variables.

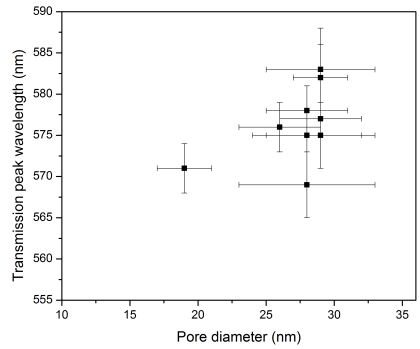

(a) Set 1.1

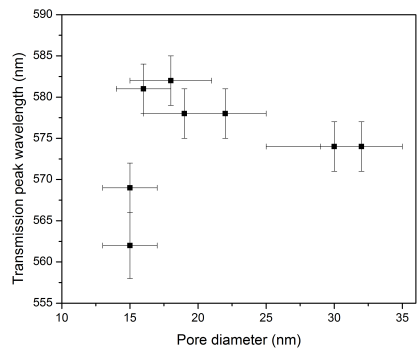

(b) Set 1.2

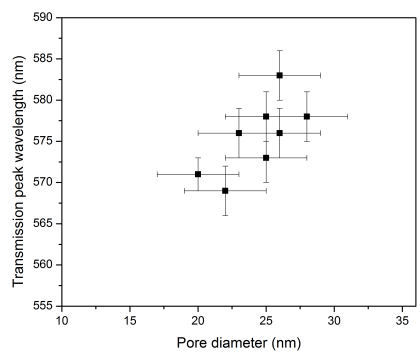

(c) Set 1.3

Figure 2.10: Peak wavelength versus pore diameter. Also here, there is no clear correlation between these variables.

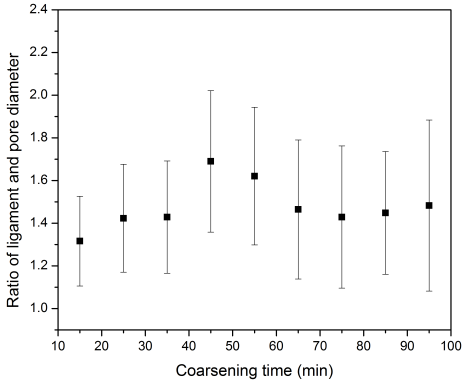

(a) Set 1.1

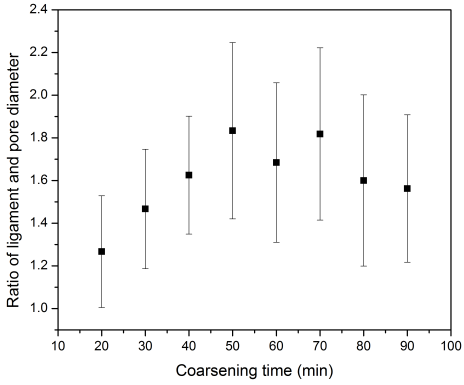

(b) Set 1.2

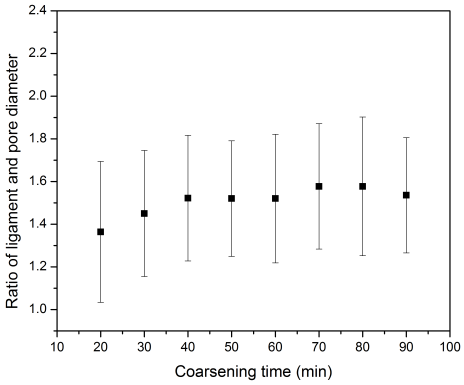

(c) Set 1.3

Figure 2.11: The plots of the ratio of ligament and pore diameter dL/dP versus coarsening time in minutes. Not much can be said about this, since unfortunately the errors are too big.

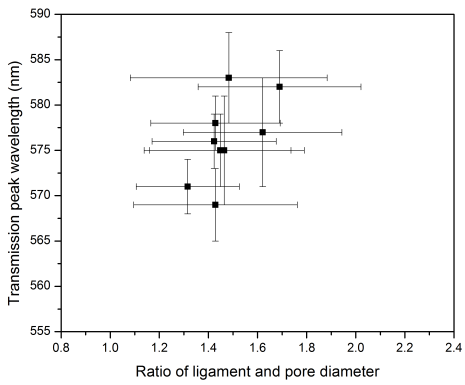

(a) Set 1.1

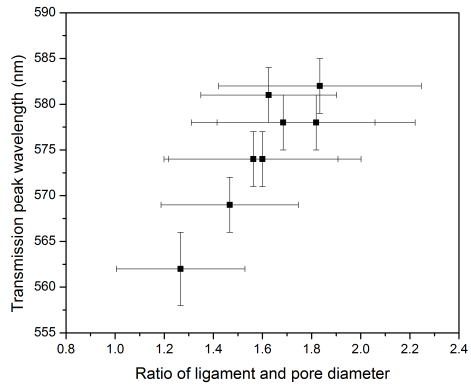

(b) Set 1.2

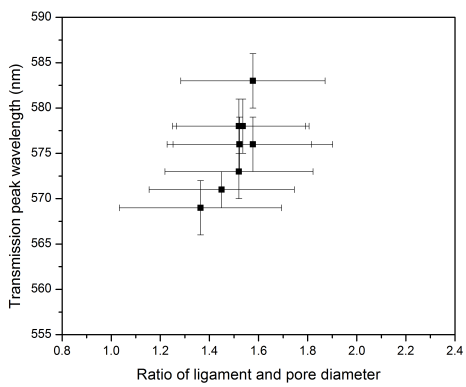

(c) Set 1.3

Figure 2.12: The plots of the transmission peak wavelentgh versus the ratio of the ligament and pore diameter dL/dP. Only set 1.2 seems to show some correlation, but since this is absent in the other two sets, this is no hard evidence.

2.4 Comparison with theory

A few theories exist for calculating the absorption/transmission spectrum of plasmonic metal structures. Mie theory does this for spherical metal nanoparticles in a dielectric medium. It uses the complex dielectric function of both the metal and the surrounding medium to do this [8]. A modification of this theory, called Mie-Gans theory, does the same, but for rod-shaped nanoparticles [8].

The structure of the ligaments in nanoporous gold resembles that of a network of interconnecting nanorods (see figures 1.1 and 1.2). It would be interesting to look for similarities between predictions made by this theory and the experimentally obtained transmission spectra of the NPG. However, Mie-Gans theory does not allow the nanoparticles to touch each other.

The **Bruggeman (BM) effective medium theory**, on the other hand, does. Detsi has investigated this theory for the case of gold nanorods [8]. In the following section, the Bruggeman effective medium theory will be presented together with a way to calculate the transmission spectrum for different nanoparticles. Also, a simulation has been made for a few situations in order to make a comparison between the theory and the experimental data possible.

2.4.1 Bruggeman effective medium theory

The refractive index n and the absorption coefficient k are related to the complex dielectric function ε of the material [9][10][11] by the following equation:

$$\varepsilon = (n + ik)^2 = \varepsilon' + i\varepsilon'' \tag{2.1}$$

In this equation, ε' is the real part and ε'' the imaginary part of the dielectric function. If one is able to determine ε' and ε'' of a material, the refractive index and the absorption coefficient can be calculated. With n and k known, the transmittance T can be computed using the following equation [11]

$$T = \left[1 - \frac{(n-1)^2 + k^2}{(n+1)^2 + k^2}\right]^2 \exp\left(\frac{-4\pi k d}{\lambda}\right) \tag{2.2}$$

Here, d is the thickness of the material and λ is the wavelength of the incoming light. Since both the real and imaginary part of the dielectric function depend on the wavelength λ , n, k and also T depend on λ.

With the transmittance T known, the absorbance A can be calculated with the following equation:

$$A = -\log_{10}(T) \tag{2.3}$$

For most pure materials such as water [12] and gold [13] (see figure 2.13) the complex dielectric functions are well-known, see figure 2.13.

For composite materials however, the dielectric function can be found using the Bruggeman Effective Medium Theory. The effective dielectric function of the composite material is calculated using the following equation[10]:

$$f_m \frac{\varepsilon_m - \varepsilon_{eff}}{\varepsilon_m + \kappa\varepsilon_{eff}} + f_w \frac{\varepsilon_w - \varepsilon_{eff}}{\varepsilon_w + \kappa\varepsilon_{eff}} = 0 \tag{2.4}$$

In Eq. (2.4) ε_{eff} is a function of the complex dielectric functions of the metal (ε_m) and of the surrounding medium, in this case water (ε_w), the screening parameter κ which will be explained shortly, and f_m and f_w, the volume fractions of the metal and the surrounding medium respectively. The following holds for the volume fractions:

$$f_m + f_w = 1$$

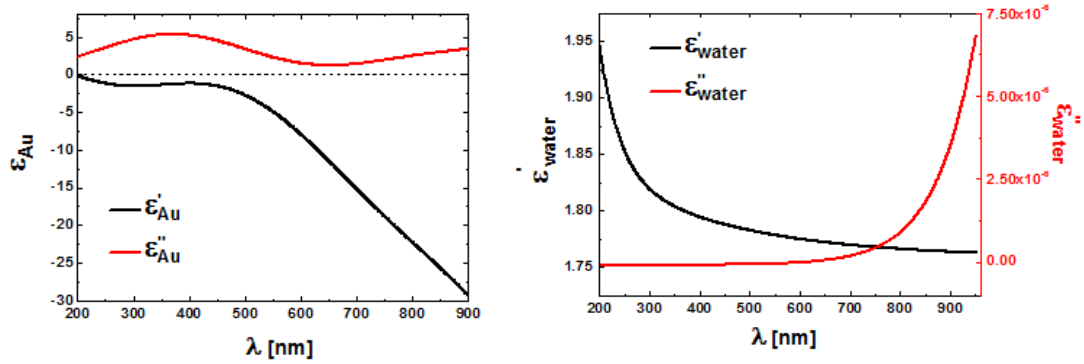

(a) Gold (b) Water

Figure 2.13: The real and complex components of the dielectric functions of gold and water. Plots from [8].

Since f_m is a measure of the relative density in a nanoporous metal, it is different for different feature sizes. It was shown earlier that ligaments and pores do not grow at equal rates, which suggests that also the relative density does not stay constant. A recent article by Detsi et al. [14] shows that the volume fraction f_{m} can be approximated by:

$$f_m \sim \frac{1}{AR} \tag{2.5}$$

where AR (aspect ratio) is the ratio between the pore diameter and the ligament diameter (see also figure 2.16):

$$AR = \frac{\text{length of ligament}}{\text{diameter of ligament}} \tag{2.6}$$

The screening parameter κ from Eq. (2.1) is a function of the shape of the nanoparticles under investigation and also depends on the orientation of the nanoparticle relative to the electric field of the incoming light. When looked at the samples of NPG, the ligaments resemble nanorods in contact with each other. Therefore it is decided to view the ligaments as if they were nanorods.

κ is calculated using the following equation [9][10][11]:

$$\kappa_j = \frac{1 - P_j}{P_j} \tag{2.7}$$

Here, P_j is the depolarization factor, with $j \in [A, B, C]$, where A, B, C represent the three axes of the particle, and $A > B = C$. For these axes, the following equations are used to calculate P_j:

$$P_A = \frac{1 - e^2}{e^2}\left[\frac{1}{2e}\ln\left(\frac{1+e}{1-e}\right) - 1\right] \tag{2.8}$$

$$P_B = P_C = \frac{1 - P_A}{2} \tag{2.9}$$

In both equations, the parameter e is a function of the aspect ratio AR [9]

$$e^2 = 1 - \frac{1}{AR^2} \tag{2.10}$$

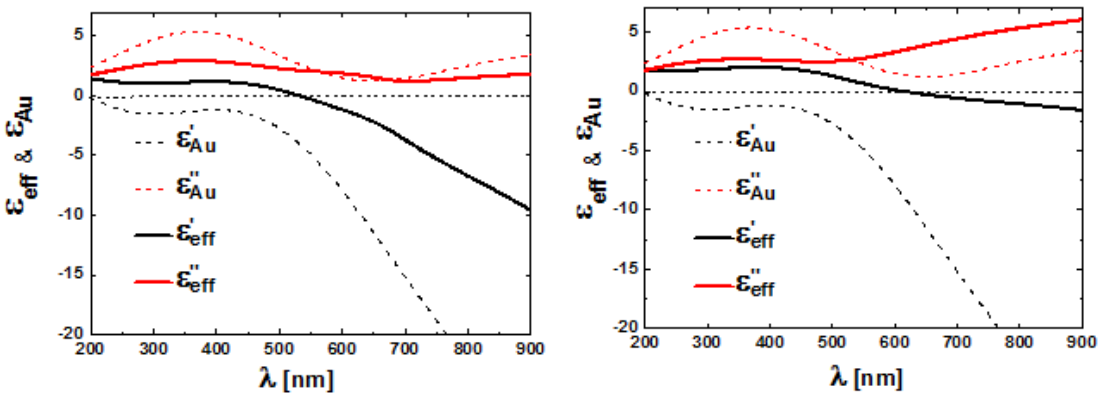

(a) Central axis oriented along electric field

(b) Central axis oriented perpendicular to electric field

Figure 2.14: The real and complex components of the effective dielectric function (solid curve) plotted with the dielectric function of pure gold (dashed curve) for different orientations of the principal axis of the nanorod. Plots from [8].

With the aspect ratio AR known, κ_j and κ are known and therefore ε_{eff} can be calculated. To do this, first Eq.(2.1) is rewritten into quadratic form:

$$\kappa_j \varepsilon_{eff,j}^2 - [\varepsilon_m(f_m\kappa_j - f_w) + \varepsilon_w(f_w\kappa_j - f_m)\varepsilon_{eff,j} - \varepsilon_m\varepsilon_w = 0 \tag{2.11}$$

Using Eq. (2.11), one can find the solutions for this equation, which has been done by Detsi [8]. For each j, one of these solutions appears to be the physical solution and can be used to calculate the $\varepsilon_{eff,j}$ for all the λs in the visible range. A typical solution of this equation, using the parameters of the NPG/water composite material, has been plotted in figure 2.14 together with the dielectric functions of pure gold. Note that the orientation of the nanofeatures is of importance to ε_{eff}.

Now that the ε_{eff} is known for λ in the visible range, the refractive index n and the absorption coefficient k can be calculated. Eq. (2.1) has been rewritten into the following equations:

$$n_{eff}^2 - k_{eff}^2 = \varepsilon'_{eff} \tag{2.12}$$

$$2n_{eff}k_{eff} = \varepsilon''_{eff} \tag{2.13}$$

From these equations, n_{eff} and k_{eff} can be calculated in the following way:

$$n_{eff} = \frac{1}{\sqrt{2}}\sqrt{\varepsilon'_{eff} + \sqrt{\varepsilon'^2_{eff} + \varepsilon''^2_{eff}}} \tag{2.14}$$

$$k_{eff} = \frac{\text{sign}(\varepsilon''_{eff})}{\sqrt{2}}\sqrt{-\varepsilon'_{eff} + \sqrt{\varepsilon'^2_{eff} + \varepsilon''^2_{eff}}} \tag{2.15}$$

Now the transmittance T and absorbance A can be computed by filling in n_{eff} and k_{eff} in Eqs. (2.2) and (2.3). The result of T is shown in figure 2.15.

When looking at these results, a few things can be observed:

- When the principal axis (A) of the nanorods (or ligaments) is oriented perpendicular to the electric field of the incoming light, a short-wavelength transmission peak emerges.

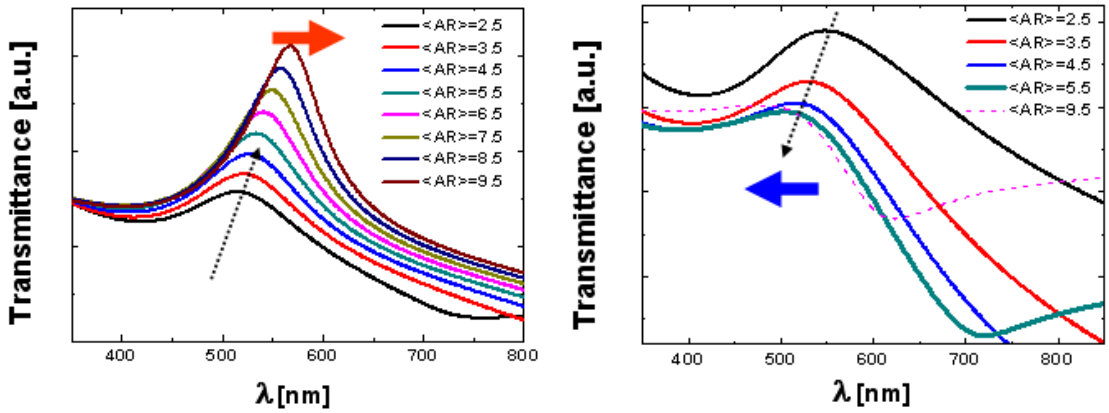

(a) Central axis oriented along electric field

(b) Central axis oriented perpendicular to electric field

Figure 2.15: The simulated transmission spectra plotted for different aspect ratios. Plots from [8].

- A long-wavelength peak is found when the principal axis is oriented parallel to the electric field of the light.
- When the AR is increased, the long-wavelength peak shifts towards longer wavelengths (into the red) while the short-wavelength transmission peak shifts to shorter wavelengths (into the blue).
- Increasing the thickness of the film only influences the intensity of the spectrum, not the positions of the peaks.

These observations ask for a fresh look at the gathered data, to see if these phenomena are also observed in our samples. However, more experiments should be done to confirm this, see section 3.7.

2.5 Discussion

After the work of E. Detsi [8] on Bruggemans Effective Medium Theory, the same spectra and the same samples could be used, but instead of pore diameter, the ligament length should be measured, to calculate the aspect ratio AR, which we define as the ratio of the average ligament length to the average ligaments diameter. In figure 2.16 a short first result is presented to indicate some of the observations done on the simulations can also be done on the NPG/water samples.

- The short-wavelength transmission peak shifts slightly to the blue for increasing AR.
- The long-wavelength transmission peak shifts to the red for increasing AR.

These observations indicate that the Bruggeman Effective Medium Theory might very well be a good method to predict the transmission spectrum of nanoporous metals in a surrounding medium.

2.6 Conclusion

The transmission spectrum of thin nanoporous gold films was studied. More specifically, the connection between the peak wavelength of the two transmission peaks and the nanostructural properties

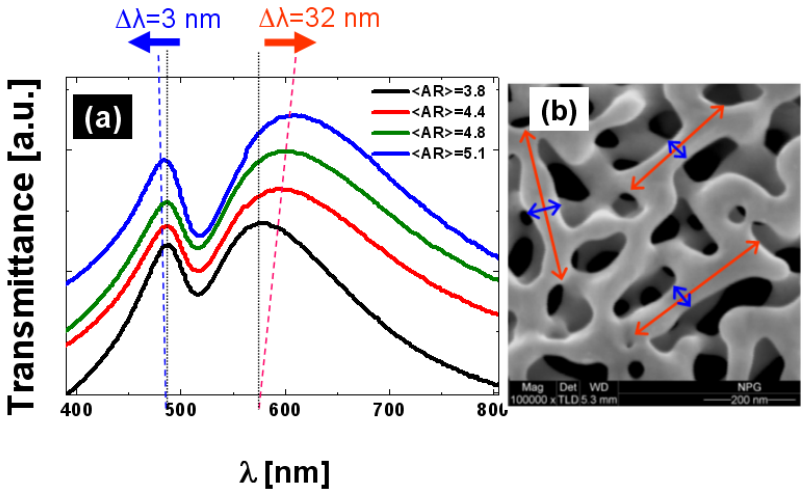

Figure 2.16: (a) First indication that indeed the aspect ratio AR is important for the position of the transmission peak [8]. For an increasing aspect ratio, the right peak continuously shifts into the red, while the left peak shifts slightly into the blue. (b) Definition of the aspect ratio of ligaments in NPG [8].

was investigated. NPG films were synthesised by de-alloying white gold leafs in acid. The feature sizes were tuned by coarsening the NPG in acid as well. No linear correlation was found between the peak wavelength and the ligament diameter, the pore diameter or the ratio of the two. After examining the Bruggeman Effective Medium Theory it was discovered that the aspect ratio AR could be the important variable for the peak wavelength. A short check of the correlation between peak wavelength and AR is in agreement with this discovery. However, more research is needed to confirm this.

2.7 Recommendations

Data fitting

For this report, the position of the transmission peaks has been determined manually. However, data-analysis software is better than the naked eye when it comes to smoothing a curve and determining its maximum. In addition to this, it is possible to fit a predefined function. In this case, the function could for example consist of the sum of two Gaussians. This way, the interference from the peaks with each other could be eliminated and both peak wavelengths could be measured more accurately.

Statistics and Automation of Micrograph Analysis

Experimental data are more credible when they can be reproduced. Also, better statistics (more data) provides a better validation for any conclusions. In this project, the data were collected by hand. It was a very time-consuming process, as all feature dimensions had to be measured manually. This was the biggest bottleneck for obtaining more data. If this could be done automatically, far more data can be generated and this phenomenon on NPG can be researched far more thoroughly.

At the same time as this project was running, another bachelor student (S. Folkersma) was looking into software that could be used to do exactly this. From 3 pictures of a NPG sample, this software was supposed to be able to construct a partially 3D-image of the nanostructure, which would

allow for ligament and especially pore diameter measurements by a computers (see section[BLAAT]). However, due to some software drawbacks, that project yielded no results useful to this project.

Another method for obtaining data from pictures is Fast Fourier Transform analysis [15][16]. When such a transform is performed on a picture with repeating features, the Fourier spectrum contains information about the sizes of recurring features in the picture. A little time has been spent during this project to look into this method, but to avoid the project becoming to broad, it was decided this was something for the recommendations.

References

[1] A. Trügler. "Optical Properties Of Metallic Nanoparticles". PhD thesis. University of Graz, 2011.

[2] X. Lang, P. Guan, et al. "Localized Surface Plasmon Resonance of Nanoporous Gold". In: *Applied Physics Letters* (2011).

[3] M. Mrejen, A. Israel, et al. "Near-Field Characterization of Extraordinary Optical Transmission in Sub-Wavelength Aperture Arrays". In: *Optics Express* (2007).

[4] L. de Jeer. "Light Induced Hydrogen Evolution on Nanoporous Gold Film". MA thesis. University of Groningen, 2013.

[5] E. Detsi et al. "Direct Sythesis of Metal Nanoparticles with Tunable Porosity". In: *Journal of Material Chemistry* (2012).

[6] E. Detsi et al. "Fine-Tuning the Feature Size of Nanoporous Silver". In: *Crystal Engineering Communications* (2012).

[7] Y. Ding, Y. Kim, et al. "Nanoporous Gold Leaf:"Ancient Technology"/Advanced Material". In: *Advanced Materials* (2004).

[8] E. Detsi. "Metallic Muscles: Enhanced Strain and Electrolyte-Free Actuation". PhD thesis. University of Groningen: Zernike Institute for Advanced Materials, 2012.

[9] S Link and M.A. El-Sayed. "Shape and Size Dependence of Radiative, Non-Radiative and Photothermal Properties of Gold Nanocrystals". In: *International Reviews in Physical Chemistry* (2000).

[10] C.A. Foss Jr, G.L. Hornyak, et al. "Template-Synthesized Nanoscopic Gld Particles - Optical Spectra and the Effects of Particle Size and Shape". In: *Journal of Physical Chemistry* (1994).

[11] C.A. Foss Jr, M.J. Tierney, et al. "Template Synthesis of Infrared-Transparent Metal Microcilinders: Comparison of Optical Properties with the Prediction of Effective Medium Theory". In: *Journal of Physical Chemistry* (1992).

[12] G.M. Hale and M.R. Querry. "Optical Constants of Water in the 200-nm to 200-μm Wavelength Region". In: *Applied Optics* (1973).

[13] P.B. Johnson and R.W. Christy. "Optical Constant of Noble Metals". In: *Physical Review* (1972).

[14] E. Detsi et al. "On the Specific Surface Area of Nanoporous Materials". In: *Acta Materialia* (2011).

[15] T. Fujita and M.W. Chen. "Characteristic Length Scale of Bicontinuous Nanoporous Structure by Fast Fourier Transform". In: *Japanese Journal of Applied Physics* (2008).

[16] T. Fujita, L. Qian, et al. "Three-Dimensional Morphology of Nanoporous Gold". In: *Applied Physics Letters* (2008).

Appendix A

De-alloying

The experimental procedure of de-alloying was as follows:

1. a gold leaf was carefully placed into a glass Petri dish.
2. water was carefully introduced beneath the leaf. This was done to make sure the acid, while it is being introduced, spreads across the leaf's surface rapidly. This would make the leaf de-alloy in a more homogeneous way, instead of de-alloying faster or having a head start where the acid was first introduced.
3. the acid was carefully introduced, while keeping safe distance from the leaf with the pipette to avoid bending or breaking the sample, as it is already rapidly de-alloying at this stage. After this step, the leaf floats on the acidic solution, see figure A.1.
4. this step is optional: if the coarsening was done in the same solution as de-alloying, the leaf can remain in the acid, see Appendix B. For other methods, the leaf had to be washed. This means the acid was carefully removed before repeatedly water was introduced and removed from the Petri dish, to dilute and take away most of the acid and dissolved silver.

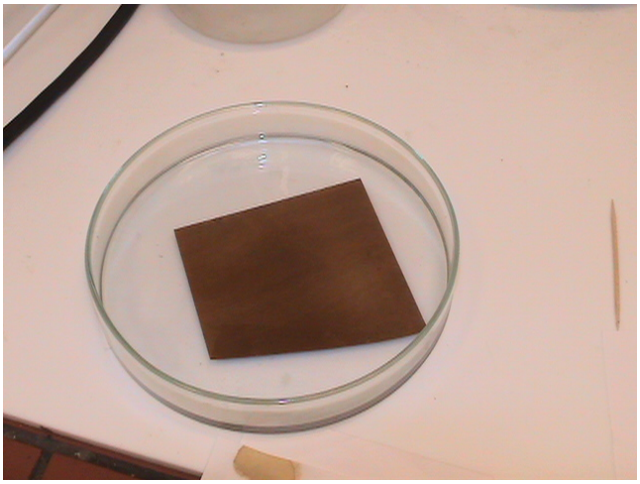

Figure A.1: A white gold leaf in a Petri dish with acid. Noting by the brown colour, the leaf has been dealloyed. Most of the silver is gone and the sample is nanoporous.

Appendix B

Coarsening Methods

There exist a number of ways of coarsening the microstructure of a nanoporous metal [8]. Nanoporous gold has a large surface area. It 'would like to' reduce its surface energy by reducing its surface area [8]. Usually this is a very slow process, as the gold atoms are not very mobile at room temperature. However, if the temperature is increased, the atoms become more mobile and the sample coarsens faster. Also, if the surface energy is increased, for example by applied a potential to the NPG or by placing the sample in an acidic solution, the NPG also coarsens.

During the FIT-internship the methods incorporating heat and acid were explored.

Thermal coarsening in the oven

Initially, the idea of the project was to put a sample of NPG in the oven to coarsen it for a while before obtaining the transmission spectrum as well as a SEM sample. After all this, the same sample would be put back in the oven to repeat the entire procedure. This way, all measurements would be done on the same piece of NPG.

However, as was be explained in section 2.3.1, the measured transmission spectra are a lot better when the pores are filled with water. It is difficult to bring water into the pores of the NPG if the sample is not sandwiched between two glasses, as in section 2.2.2. This is mainly due to the water forming droplets that tear up the brittle NPG film as the droplet moves under the sample.

To solve this problem, a second glass plate was placed on top of the sample. The NPG was now sandwiched between the two plates, rendering it immobile, thus making it less likely to deform or crack. Introducing water is simple now, since the plates are close enough enable capillary absorption. Whenever this is performed, the water can be observed to slowly enter the sample.

However, by choosing to use this method, it becomes almost impossible to do coarsening in the oven. Or actually, to do multiple stages of coarsening on the same sample. In order to take a SEM sample for every coarsening step, the top glass plate has to be taken off to be able to reach the NPG film. Removing a plate without affecting the sample is difficult: the slightest shear movement destroys the sample. Relying on a single sample for all your measurements is risky, since every time the glass plate has to be removed, there is the chance the process destroys the structure. Therefore a different method of coarsening was chosen.

Chemical coarsening in nitric acid at room temperature

The main method of coarsening the NPG that was employed during this project was to keep the leaf in the same acid as in which it was de-alloyed. At different times a piece of the large de-alloyed gold leaf was taking out and put on glass. Of each of these samples, the transmission spectrum was measured and a SEM sample was taken for examination in the electron microscope as explained in section 2.2.2. Afterwards, all samples were kept and stored.

This method made it possible to have a different sample for every coarsening step. Since every sample only had one coarsening step and would only provide one SEM sample, a second glass plate could be introduced. However, using this method also meant that each sample would be a different part of the larger gold leaf.

For this method, after the first three steps described in Appendix A, the procedure of obtaining samples was as follows:

1. a toothpick was used to puncture the de-alloyed gold leaf to define the edge for the sample. Enough punctures along the preferred boundary would break the sample from the leaf along this boundary without influencing the main surface of the sample.

2. with a pair of tweezers, a small piece of glass was taken [picture moet nog?] and was used to scoop up the freely floating sample from the solution.

3. the sample was put in a glass cup containing demineralised water. It was kept here for 5 minutes. This allowed the solution of acid and silver to diffuse from the pores into the large volume of water.

4. the sample was placed on a nice spot on the glass microscope glass, somewhat like figure 2.2.

5. after this, the sample was left to dry before introducing the other glass plate.

Coarsening on hot water and hot nitric acid

It was also tried to coarsen the NPG on hot water. This was a compromise between the thermal coarsening in the oven, which had to be done on a solid glass plate, and the 'freestanding' property of chemical coarsening. There were only a few attempts that all failed. The NPG film showed a rough surface while afloat, which would crack as it would dry on the glass.

Of course, one can also try to combine the heat with the chemical coarsening. After the experiments of this project had been finished, Detsi made a few samples on hot acid ($\sim 75\,^{\circ}$C). This seemed to work pretty well, coarsening the samples to contain ligaments of $\sim$ 60nm in diameter in only 2 hours. For future projects, this could be a nice way to tune feature size.

Chapter 3

Photo-electrochemical Properties of Nanoporous Gold (Bachelor Research)

3.1 Introduction

3.1.1 Solar devices

With fossil fuels growing increasingly scarce in the near future, the search for renewable energy is stronger than ever. As the Earth's most abundant and accessible source of energy, sunlight is one of the potential suppliers of renewable energy. Solar cells are great for generating electricity and are used more and more to generate electricity.

However, at night it is dark and these solar cells do not generate any power, but there is still a demand for energy. Creating a device that produces hydrogen from water would solve this problem, as the hydrogen can be stored for usage during the night. Both sunlight and water are abundant, making such a device interesting for renewable energy [1][2]. Such devices exist, but they are made from very expensive materials and require highly corrosive electrolytes, which makes it difficult to use for substantial hydrogen production (as a large surface is needed to collect sunlight)[3][2]. Also, cheaper devices have been created, but they only the UV-light from the spectrum, which is only a very small fraction of the the total irradiation [4].

Metal nanoparticles have been shown to enhance the photoinduced water splitting of semiconductor cells in a number of ways [1][2][4]. It would be interesting to see if nanoporous metals provide the same enhancements or can even drive water splitting themselves, without the help of a semiconductor.

3.1.2 Objectives

The aim of the Bachelor project was to develop theoretical support for the experimental works of De Jeer (Master Thesis, see [5]) and Detsi (Postdoctoral Project). Before the focus of the experiments came to lie with water splitting and hydrogen production, it lay with the conversion of light into electrical energy. This direction gradually changed to water splitting.

At first, the goal was to build a device that would convert solar energy into electrical energy. This was to be done with NPG and organic semiconductors, see figure 3.1. The NPG would provide the electrons or holes while the semiconductor would take care of the charge separation, see figures 1.10 and 1.11. However, the organic semiconductor brought along several difficulties.

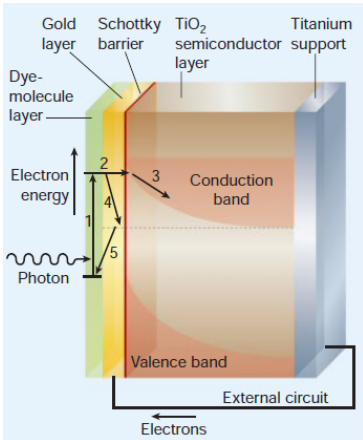

Figure 3.1: Solar cell generating electricity [6]. The electrons from the dye molecule enter the conduction band of the TiO_2 and flow through the electric circuit to enter the dye molecule again. The initial idea of this project was to build a similar device, but without the dye-molecules. The gold would be nanoporous and would be generating its own hot electrons.

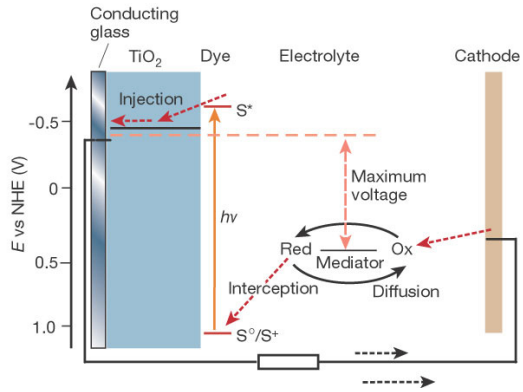

Figure 3.2: Schematic of dye-sensitized solar cell. The dye is excited by a photon and passes the electrons to the conduction band of the semiconducting TiO_2. A redox mediator in the electrolyte delivers electrons to the oxidized dye molecule and is in turn reduced again by the electrons that flow from the circuit [7].

Therefore, a theoretical attempt was made to come up with a cell similar to a dye-sensitized solar cell: the NPG would inject electrons or holes into a redox mediator in solution, see figure 3.2. In this figure the NPG would take the place of the dye molecule. However, this approach would also require a semiconductor material and a suitable redox mediator.

Before these were found, the goal of the project was changed again. Now the focus came to lie with water splitting, see figure 3.6. As water splitting on gold nanoparticles had already been reported to work, the step to nanoporous gold could prove simpler than the previous goals of this project. Also, the electrolyte of such a cell would be simple water or an alkaline or acidic solution, no special redox mediator.

The work described in this chapter is the work done for this final goal: constructing an NPG-based photo-active water splitting device.

3.1.3 Outline of Chapter

This chapter, discussing the main work of the Bachelor project, will be built up chronologically. By doing so, it can be understood how the experiments came to be.

- In *Background* (section 3.2) the information required to understand the motivation for the setup of experiment 1 (section 3.3) is provided. This information consists of an explanation of redox reactions, the Nernst reaction, the water splitting reactions themselves and devices
- *Experiment 1* (section 3.3) describes the experimental setup, the results of the experiment and a discussion of the results.
- As the experimental results cannot be adequately explained by the principles discussed in the background information, *Required Considerations* (section 3.4) provides the theory to better understand the experimental results of Experiment 1. This section will discuss the working

principles of operational cells since the Background information only provided a description of static (non-operational) cells). With this addition to the theory, a mechanism will be proposed that could explain the results of experiment 1 better.

- With this addition to the theory, in *Proposed Mechanism* (section 3.5) a mechanism will be proposed that could explain the results of experiment 1 better.

3.2 Background

3.2.1 Redox Reactions

In order to understand water splitting and the experiments that were performed and discussed later on in this report, it is important to understand the phenomenon of redox reactions. "A redox reaction is a reaction in which there is transfer of electrons from one species to another" [8]. The reaction consists of two half-reactions: 1) an oxidation reaction, where electrons are removed from a material, and 2) a reduction reaction, where electrons are added to a material. The electron donating material is called the reductant (or reducing agent) and the electron accepting material is called the oxidant (or oxidizing agent). The reduced species and oxidized species in a half-reaction are called a redox couple. Such a redox couple and half reaction is often written down as [8][9]:

$$\mathrm{Ox} + ze^- \rightleftharpoons \mathrm{Red} \tag{3.1}$$

where z is the number of electrons donated or accepted, depending on the direction of the reaction (to the left→ donation/oxidation; to the right→acceptance/reduction). An example of such a redox reaction and its half-reactions is given below. In a system containing solid copper and zinc, and their respective ions, the half-reactions are [10]:

$$\mathrm{Cu}^{2+}(aq) + 2e^- \rightleftharpoons \mathrm{Cu}(s)$$
$$\mathrm{Zn}^{2+}(aq) + 2e^- \rightleftharpoons \mathrm{Zn}(s)$$

Since copper ions are a stronger reductant than zinc ions, and zinc is a stronger oxidant than copper (see section 3.2.2), this is the redox reaction that will take place:

$$\mathrm{Cu}^{2+}(aq) + \mathrm{Zn}(s) \rightleftharpoons \mathrm{Cu}(s) + \mathrm{Zn}^{2+}(aq)$$

It is observed that solid zinc dissolves, while the copper ions form a solid.

Such a reaction does not have to be a direct contact; for the two half-reactions to occur, the two materials only have to be in electrical and ionic contact. An example of this is a Daniel cell (figure 3.3). The electrons can flow from the oxidant to the reductant through the electrocal contact, while the change in charge near the surface of the electrode is compensated by a flow of ions in the solution. The potential difference between the two electrodes is called the cell potential. The higher the cell potential, the more work an electrode can do when flowing from the one to the other electrode. If the overall redox reaction is in equilibrium, the cell can do no work and the cell potential is equal to zero [8].

3.2.2 Nernst Equation

Reactants undergo a reaction if the products of the reaction are in an energetically favoured state. Whether this is the case for a certain reaction is described by the Gibbs free energy $\Delta_r G$ of that specific reaction. The Gibbs free energy provides information about how much work can be done by a system, and its sign tells one whether the reaction is spontaneous or not [8]:

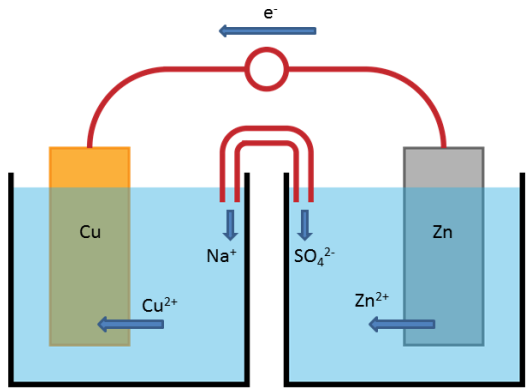

Figure 3.3: Daniell Cell [11][9]. Zinc dissolves and copper solidifies while the electrons flow through the electrical circuit. The salt bridge compensates for the changes in charge in the solution.

$$\text{if}\,\Delta_r G = \begin{cases} < 0 & \text{the reaction is spontaneous} \\ = 0 & \text{the reaction is in equilibrium} \\ > 0 & \text{the reverse reaction is spontaneous} \end{cases} \tag{3.2}$$

The Gibbs energy depends on the composition of the reaction mixture [8][9]:

$$\Delta_r G = \Delta_r G^{\ominus} + RT \ln Q \tag{3.3}$$

with $\Delta_r G^{\ominus}$ being the standard reaction Gibbs energy, R the gas constant and T the temperature [8].

Q is the reaction quotient [8][9]:

$$Q = \frac{\prod_i a_i^{\nu_i}}{\prod_j a_j^{\nu_j}} \tag{3.4}$$

where a_i is the activity (see [8]) of product i and a_j is the activity of reactant j, both raised to the power of ν, which is the stoichiometric coefficient of the respective product or reactant.

Since the Gibbs energy is related tot the amount of work a system can do, it is also related to the cell potential [8][9]:

$$-nFE = \Delta_r G \tag{3.5}$$

Here, F is Faraday's constant and n is the number of electrons transferred in a reaction [8]. Using this relation, one can derive the **Nernst equation** from Eq. (3.3):

$$E_{cell} = E_{cell}^{\ominus} - \frac{RT}{zF} \ln Q \tag{3.6}$$

with

$$E_{cell}^{\ominus} = -\frac{\Delta_r G^{\ominus}}{nF} \tag{3.7}$$

The Nernst equation expresses the cell potential in terms of the composition of the cell. At standard conditions and equilibrium, Q is equal to K, which is the equilibrium constant of a reaction. In equilibrium, a cell cannot do work, so $E_{cell} = 0$.

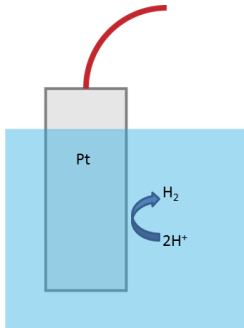

Figure 3.4: Standard Hydrogen Electrode (SHE)

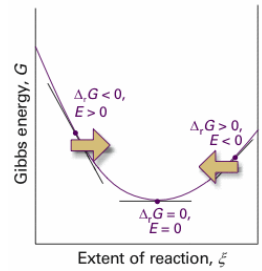

Figure 3.5: A spontaneous reaction occurs in the direction of decreasing Gibbs energy[8]

A similar derivation can be done for the potential of one of the half-reactions. One will arrive at the following equation:

$$E_{red} = E^{\ominus}_{red} - \frac{RT}{zF} \ln Q \tag{3.8}$$

with Q containing the activities of the components of the half-reaction instead of the full redox reaction. Since the cell potential is the potential difference between the two redox electrodes at which the half reactions take place, E_{cell} is the sum of both electrode potentials:

$$E_{cell} = E_{red} - E_{ox} \tag{3.9}$$

and also

$$E^{\ominus}_{cell} = E^{\ominus}_{red} - E^{\ominus}_{ox} \tag{3.10}$$

It is not possible to measure the potential of a single electrode, but it is possible to measure electrode potentials relative to each other [8][12]. This has been done by defining the standard hydrogen electrode (SHE), which is a platinum electrode accommodating the half-reaction of hydrogen (see figure 3.4) [8]:

$$2\mathrm{H}^+(aq) + 2\mathrm{e}^- \rightleftharpoons \mathrm{H}_2(g) \quad \mathrm{E}^{\ominus} = 0.00V$$

It has been set to $0.00V$ for all temperatures, under standard conditions, which means the concentration of H^+ is equal to $1ML^{-1}$ ($pH = 1$) and the fugacity (or pressure) of H_2 is 1 bar [8]. Most redox potentials are expressed relative to the SHE by using Eq. (3.10). Other reference electrodes are used, but these only define a different point of origin ($E = 0$).

With the standard reduction potentials (SRPs) known for most redox couples (see [10]), one can start designing galvanic and electrolytic cells. Remember that the sign of $\Delta_r G$ holds information on the spontaneity of the reaction. By using Eq. (3.5), for E_{cell} this turns into:

$$\text{if } E_{cell} = \begin{cases} > 0 & \text{the reaction is spontaneous} \\ = 0 & \text{the reaction is in equilibrium} \\ < 0 & \text{the reverse reaction is spontaneous} \end{cases} \tag{3.11}$$

See also figure 3.5.

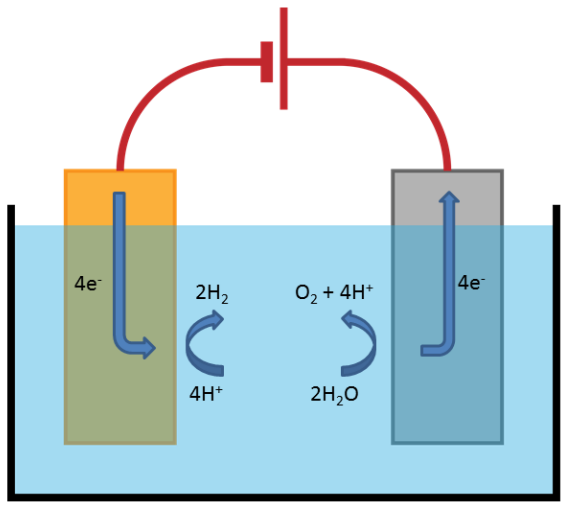

Figure 3.6: Water splitting cell. For an applied potential of > 1.23V, hydrogen is produced on one electrode and water is split into protons and oxygen on the other.

3.2.3 Water splitting

The goal of the research project was to investigate whether or not it would be possible to make a water splitting device with nanoporous gold. In order to do this, first the water splitting reactions have to be understood.

Water splitting, also called electrolysis of water, is a redox reaction. The two half-reactions are the **hydrogen evolution reaction** (HER) and the **oxygen evolution reaction** (OER)[4][13][14][9]:

$$2\mathrm{H}(aq)^{+} + 2e^{-} \rightleftharpoons \mathrm{H}_2(g) \tag{3.12}$$

$$\mathrm{O}_2(g) + 4\mathrm{H}^{+} + 4e^{-} \rightleftharpoons 2\mathrm{H}_2\mathrm{O}(l) \tag{3.13}$$

Redox couple	Reduction potential (V) vs. SHE
$2\mathrm{H}^{+} + 2e^{-} \rightleftharpoons \mathrm{H}_2(g)$	0.00
$\mathrm{O}_2(g) + 4\mathrm{H}^{+} + 4e^{-} \rightleftharpoons 2\mathrm{H}_2\mathrm{O}(l)$	1.23

Table 3.1: Redox couples of HER and OER with their reduction potentials [10].

The total water splitting reaction looks like this:

$$2\mathrm{H}_2\mathrm{O} \rightleftharpoons 2\mathrm{H}_2 + \mathrm{O}_2 \tag{3.14}$$

However, since the HER is the reducing reaction and OER the oxidizing reaction:

$$E^{\ominus}_{cell} = E^{\ominus}_{red} - E^{\ominus}_{ox} = 0.00\mathrm{V} - 1.23\mathrm{V} = -1.23\mathrm{V} \tag{3.15}$$

As discussed in section 3.2.2, this means that this reaction is not spontaneous, and as discussed in section 3.2.2, a voltage higher than the cell potential E^{0}_{cell} has to be applied to let the reaction flow in the direction corresponding to water splitting: the reaction requires energy. This is discussed more in-depth in section 3.4 .

3.3 Experiment 1

The first experiment was aimed at determining whether or not plasmons in NPG are able to produce hydrogen (not water splitting). At the time on which the experiment was performed, little was known about the reaction mechanisms of electrochemical cells (section 3.4). What wás known, or at least considered to be important, was that gold had a low Fermi level, below the redox potential of the HER (see figure 3.7). It was thought that light would excite hot electrons in the NPG with an energy high enough to cross the gap between the NPG-Fermi level and the HER level and would take part in the HER reaction. The holes, left behind by the hot electrons, would be filled by the electrons generated in the oxidation of aluminium.

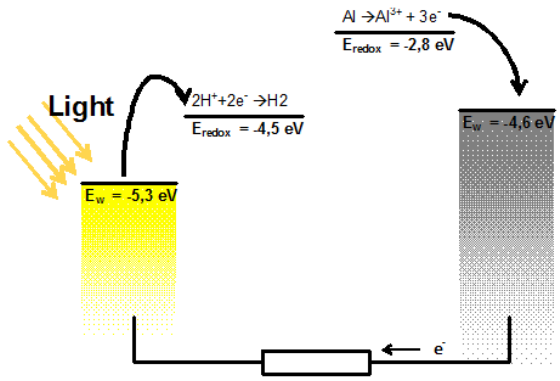

Figure 3.7: Initial perception of the working mechanism of the Al-Au cell. Hot electrons participate in the HER while the holes that are left behind are filled by electrons from the oxidizing aluminium.

See figure 3.7 for a schematic representation of the photo-electrochemical process that was thought to be the working mechanism.

3.3.1 Methods & Materials

The main experiment consisted of an electrode of NPG film, an aluminium electrode and a solution of acid. The active redox couples in this setup are shown in table 3.2:

Redox couple	Reduction potential (V) vs. SHE
$2H^+ + 2e^- \rightleftharpoons H_2(g)$	0.00
$Al^{3+}(aq) + 3e^- \rightleftharpoons Al(s)$	-1.66

Table 3.2: Redox couples of HER and aluminium with their reduction potentials [10].

The total redox reaction will be

$$2Al(s) + 6H^+ \rightleftharpoons 2Al^{3+} + 3H_2(g) \tag{3.1}$$

The cell potential under standard conditions will be $E^{\ominus}_{cell} = 1.66V$. Aluminium will spontaneously oxidize and hydrogen will spontaneously reduce.

3.3.2 Results & Discussion

The measurement of the open circuit voltage V_{oc} is shown in figure 3.8. The measurement of the short circuit current I_{sc} is shown in figure 3.9. Both are discussed below.

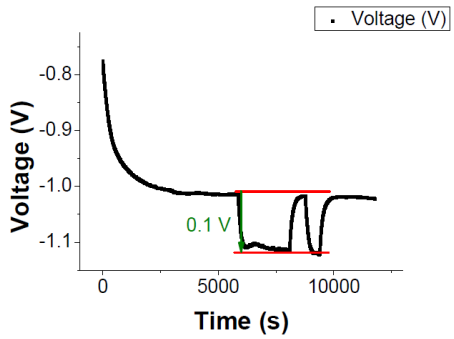

Figure 3.8: Plot of the measured voltage versus time [5]. First the cell reaches dark equilibrium (see Appendix F). Then the light is turned on and off two times. The effect is clearly visible as an increase of the cell potential. Less clear, due to the time scale, is the time the photovoltage is established, which is in the order of hundreds of seconds. Note that the sign of the voltage opposite to the calculated value. This is only due to the connections with the volt meter.

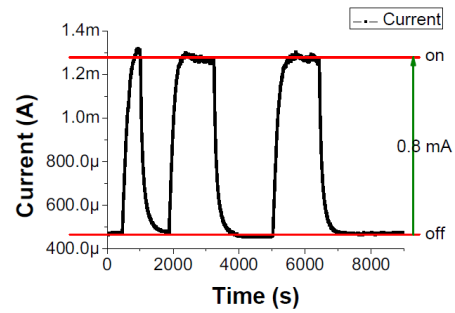

Figure 3.9: Plot of the measured current versus time [5]. The light was turned on and off 3 times. Also here, the photo-effect is clearly visible. Less clear, due to the time scale, is the time the photocurrent is established, which is in the order of hundreds of seconds. And as well as with the photovoltage, the photocurrent also takes hundreds of seconds to reach its equilibrium state.

Photovoltage

Initially, the open circuit voltage V_{oc} changes rapidly, see figure 3.8. This is due to the fact that the cell was passing current just before this measurement was started. As explained in Appendix F, the concentrations of reactants and products at the surface of the electrodes establish a new equilibrium, which takes some time. At longer times, equilibrium is reached (not regarding the illumination steps), which is not equal to 1.66V, which one would expect from the previous section. However, this can be explained by noting that this cell is a corrosion cell. A process is always taking place on the aluminium electrode, even if the cell is not doing work. This has been explained in Appendix D but requires the information in *Required Considerations*(section 3.4).

The V_{oc} changes when the NPG electrode is illuminated, see 3.8. E^0_{cell}, which is equivalent to V_{oc}, becomes more negative, which means apparently the energy level of NPG or the hydrogen couple has become more positive. Before performing this experiment, the main idea was that hot electrons reduce hydrogen. However, as can be observed in figure 3.8, it took some time for the photovoltage to establish (in the order of 10s-100s of seconds). Since the lifetime of hot electrons in nanoparticles is in the order of a few picoseconds [15], this cannot be solely the effect of hot electrons.

A solution to this might be that the equilibrium conditions of the hydrogen couple have shifted under influence of the hot electrons: as the 'concentration of hot electrons' increases, the balance of the HER (see eqs. (3.8) and (3.12)) shifts, resulting in a small amount of H_2 to be produced, leaving the NPG with less electrons. This makes the electrode more positive, which increases the difference between the NPG and the very negative aluminium, making E^0_{cell} more positive. This could be a

process on the time scale of seconds. See also section 3.4 for a more thorough investigation of this idea. Another possible solution, namely that of temperature, is discussed shortly.

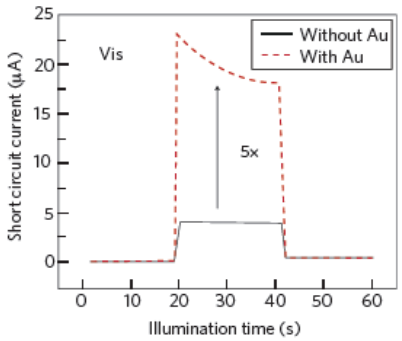

Figure 3.10: Expected behaviour of the current under illumination, if hot electrons would cause immediate reactions [4] (only the dashed line).

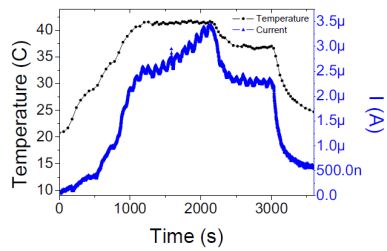

Figure 3.11: Current and temperature versus time [5]. It is observed that an increase in temperature only has a limited effect on the current.

Photocurrent

The photocurrent contradicts this process however. Figure 3.9 shows a typical plot of the closed circuit current I_{sc}. In this case, the background current is at a constant value already, in contrast with the voltage measurement of the previous section. The photocurrent is quite large with respect to the background current: there is no mistake that there is a photocurrent. However, as with the photovoltage, also the photocurrent shows a response in the order of (hundreds of) seconds. This is not what one would expect from hot electrons, which are believed to directly reduce hydrogen. A current similar to the one shown in figure 3.10 was expected, where the response is instantaneous and the current decreases afterwards to a constant value, due to the new equilibrium concentrations. This is the signal that is obtained from a semiconductor-nanoparticle composite solar water splitting material [4].

Role of Temperature

This macroscopic time scale could be explained as a temperature effect, since a change in temperature in the order of a few Kelvin of a macroscopic system also takes place at a macroscopic time scale. It has been shown that the hydrogen reaction is temperature sensitive [14], but the change is only a few millivolts per Kelvin.

Also, there has been a paper about nanoparticles producing water vapour due to the strong local heating of the water by the nanoparticle [16]. This heating could be an effect of the energy of a hot electron dissipating into the surround material by exciting other electrons. A lot of electrons will have become a little 'hotter' as effect.

However, as the ligaments in NPG are all connected, such heat is likely to be quickly distributed throughout the sample. And since the NPG is only around 100nm thick, has a large interface with electrolyte, and the lamp is only providing 0.5mW it is unlikely that the temperature of the electrode would increase by a lot.

Even so, an experiment has been performed to rule the temperature effect out completely. The entire setup was placed on a heater to raise the temperature of the electrolyte and with it the electrodes. Without illumination, the current was measured while the setup was slowly heated and

cooled, see figure 3.11. As one can see, the current follows the temperature. Nevertheless, the change in current is very small (order of μA). However, the sample is different from the one used for figure 3.9, which has a much higher background current (a factor 10^3 difference)[Why is this....? This makes them almost completely incomparable :p]. Also the aluminium electrode is heated as well in this test experiment, so the temperature dependence cannot be ascribed to the NPG electrode alone. Hence, this is no conclusive evidence that the temperature it not the main mechanism of the photocurrent. This should be investigated in a setup like the one of experiment 2 (section G.2).

The following problem does provide a bit more evidence.

Separation

The electrodes do not have to be close together. As will be explained in section 3.2.1, these redox half reactions require only an electrical contact and an ionic contact. In Experiment 1, the electrodes are very close together, only separated by a piece of filer paper. Separating the two electrodes allows for changing parameters for 1 electrode, while keeping the conditions of the other the same.

An experiments was performed under the same conditions as experiment 1, while only the electrodes had been separated and the electrolytes had been connected by a salt bridge. The result was that no longer a photocurrent was observed. Even having the two electrodes separated, but in the same electrolyte, yielded no photocurrent, while the background current, although smaller, was still present.

Another experiment brought the samples even closer. In a Petri dish, the NPG-electrode was floating on the surface of the electrolyte, while the Al-electrode was at the bottom of the Petri dish. When the distance between the electrodes was small, i.e. the NPG was above the Al-electrode, $I_{ph} \neq 0$ was observed, while $I_{ph} \approx 0$ when the electrodes were not above each other (see figure 3.12).

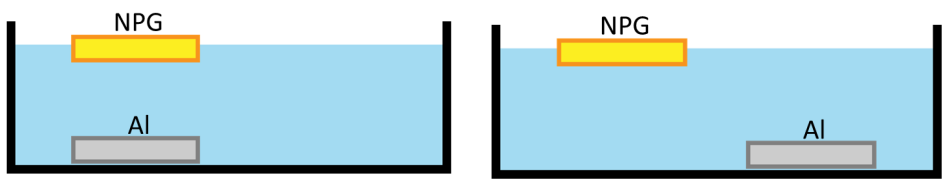

(a) Electrodes are close (b) Electrodes are far apart

Figure 3.12: Experiment to determine the effect of the electric field strength due to contact potential.

This observation provides more credible evidence that the photocurrent is no effect of the heating of the NPG, since the heating should occur at all the instances. However, nothing has been proved yet. More on this in section 3.5.

The decrease of I_{sc} for a larger distance between the electrodes is likely to arise due to the cell resistance. If ions have to travel farther, they also dissipate more of their energy into the electrolyte, raising the resistance, but this does not explain the absence of I_{ph}.

Contact Potential

If two materials with different Fermi energies E_F (see figure 3.13a) are brought into contact with each other, their Fermi levels align (figure 3.13b) [17]. In metals, this happens because the electrons in the metal with highest E_F (closest to E_{vac}) flow to the metal with the lowest E_F [18][17]. This results in the first metal to become positively charged, as it has lost electrons, and the second metal becoming negatively charged. Usually, an electric double layer forms at the interface of the two metals. However, if the metals are close to each other at some other point, an electric field arises in the gap for to the same reason (see figure 3.13c). The closer they are, the stronger the electric

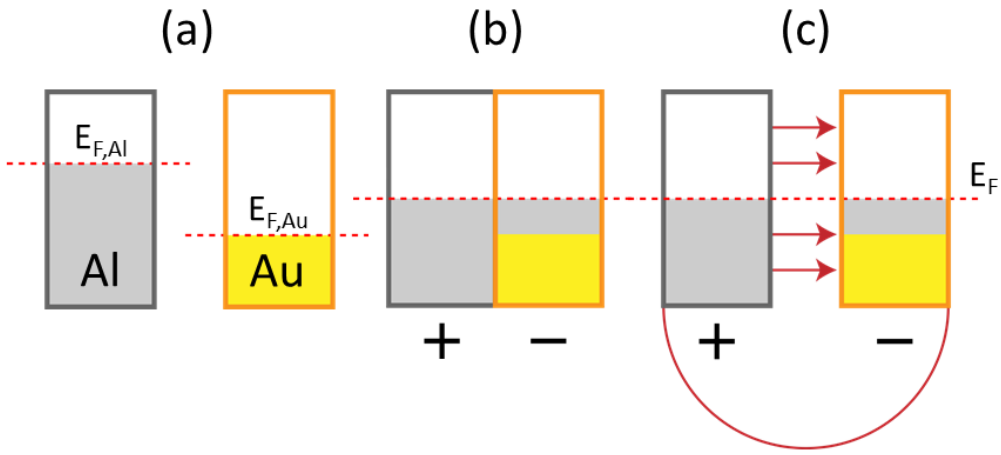

Figure 3.13: (a) Aluminium and gold with different Fermi energies; (b) In contact, electrons flow from high to low energy to align the Fermi energies; (c) In a gap between two metals in contact, an electric field establishes.

field. Since the photocurrent only appears when the electrodes are close together, it seems that this electric field is of importance.

3.4 Required Considerations

The Nernst equation (section 3.2.2) holds for static (no current-passing) cells. However, for current measurements the cell obviously ís passing current. Therefore some knowledge should be acquired regarding operational cells.

3.4.1 Electrical Double Layer, Activation Barrier and Catalysis

As already assumed in section 3.3, a Fermi level can be associated with the redox potential of a redox couple [12]. As with two metals in contact, where the Fermi levels align, this also happens for an electrode in an electrolyte [9]. Initially this is achieved by formation of an electric double layer. Ions from solution gather at the surface of the metal to compensate for the difference in Fermi levels, see figure 3.14. The simplest model of this is the Helmholtz layer, where a single layer of ions is formed of less than a nanometre from the surface [19]. This property has been utilized in capacitive devices, as this Helmholtz layer is very similar to the classical plate capacitor [9][20].

The Fermi levels can also be aligned by redox couples. If the electrode passes electrons to a reductant in solution, the electrode becomes more positive and the Fermi level drops [9] Also, if the metal itself oxidizes (as with aluminium), an excess of electrons is left behind in the metal, raising the Fermi level [9]. Or ions can adsorb on the electrode surface for a double layer to level the Fermi energy [9]. This also happens when a metal oxidizes: a layer of newly formed positive ions gather at the surface of the electrode, also forming an electrical double layer. See figure 3.14 and 3.15 for the formation and potential landscapes of these double layers.

A redox half-reaction occurs in both directions: reduction is taking place as well as oxidation. However, usually one of the two reactions dominates (see figure 3.17) or one of the components of the couple is removed from the system. In order for an oxidant atom at the surface to oxidise, it has to break free from the bonds with its neighbouring atoms and migrate through the double

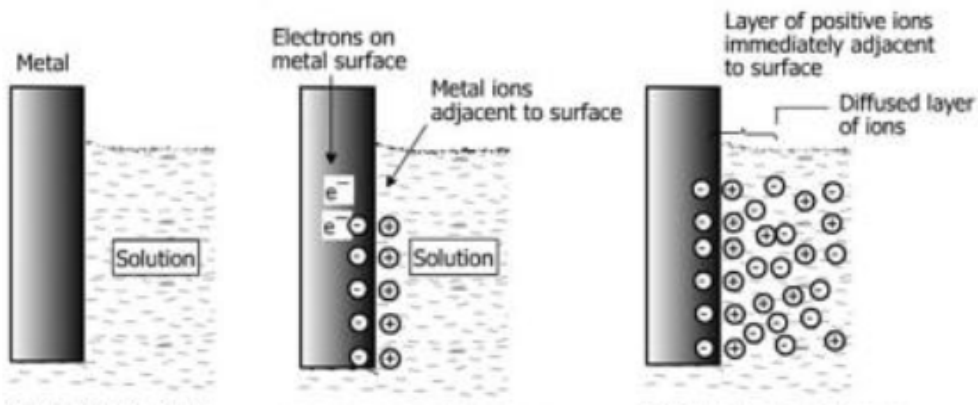

(a) At the instant of immersion

(b) First stage of formation of electrical double layer

(c) Complete double layer

Figure 3.14: Formation of electrical double layer when a metal is brought in contact with an electrolyte [9]. First a Helmholtz double layer is established (b) after which the potential landscape is smoothed by forming a diffusion layer (c). See

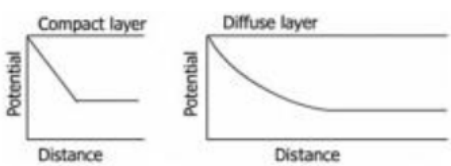

Figure 3.15: The potential landscapes of the Helmholtz double layer (left) and the diffusion/complete double layer [9]. After the Helmholtz layer is established, a diffusion layer can smooth the potential landscape.

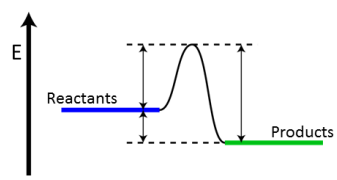

Figure 3.16: Activation barrier between reactant and product energy levels, see also [9].

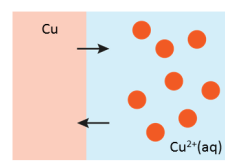

Figure 3.17: The copper redox couple. In this example, the reduction reaction dominates.

layer at the surface. Also, for an ion in solution to reduce and join the surface, it first has to cross the double layer at the surface and dispose of its solvating molecules. This means that it is an activated process; it requires some activation energy before the other state can be reached [8][9]. At temperatures far from $0K$ there are always a few ions, atoms or electrons that have more energy than the average/bulk value. Therefore, at room temperature, there are always some species that are able to cross the activation barrier. Since the reactions involve charge transfer, a current can be associated with them: a cathodic current density j_c and an anodic current density j_a, which can be described by [8][9]:

$$j_c = Fk_c[\text{Ox}] \tag{3.1}$$

$$j_a = Fk_a[\text{Red}] \tag{3.2}$$

where [Red] and [Ox] are the concentrations of reductant and oxidant, respectively. Since it is an activated process [8][9]:

$$k = B\exp[\Delta^{\ddagger}G/RT] \tag{3.3}$$

where $\Delta^{\ddagger}G_a$ represents the height of the activation barrier with respect to the level of the reactants [8]. Together with eq. (3.3), the current densities in eqs. (3.1) and (3.2) become:

$$\begin{aligned} j_a &= FB_a[Red]e^{-\Delta^{\ddagger}G_a/RT} \\ j_c &= FB_c[Ox]e^{-\Delta^{\ddagger}G_c/RT} \end{aligned} \tag{3.4}$$

where B_a and B_c are constants with units $length/second$, $\Delta^{\ddagger}G_a$ represents the height of the activation barrier with respect to the energy level of the oxidized species, while $\Delta^{\ddagger}G_c$ represents this with respect to the energy level of the reduced species, see figure 3.20 [8]. It should be noted that j_a and j_c are in opposite directions. The net current density is just the difference of the two:

$$j = j_a - j_c \tag{3.5}$$

In equilibrium, the anodic and cathodic currents balance each other, making the net current j equal to zero. Such a situation has been displayed in figure 3.18a.

The height of this **activation barrier** depends on many things. In the first place it depends on the reactants and products of the reaction itself [8]. If a reactant has to break free from a very strong bond, the activation barrier will be high. It also depends on the materials that are near the reaction site. In the case of a redox reaction taking place on an electrode, a different electrode material provides a different activation barrier for the reaction. One can imagine that the energy with which the electrons are bonded to the electrode material are of importance to a redox reaction. Materials that provide a low activation barrier for a certain reaction are said to be *catalysts* for this reaction. As can be concluded from eq. (3.4), a lower activation energy means the cathodic and anodic currents are higher (but still cancel each other out in equilibrium). This can be seen in figure 3.18b.

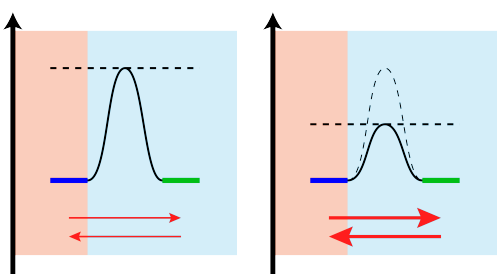

(a) The reaction is in equilibrium. The anodic and cathodic currents are equal, but in opposite direction.

(b) A catalyst lower the activation barrier of a reaction, which results in an increased cathodic and anodic current across the barrier.

Figure 3.18: Principle of catalysis explained by activation barrier height.

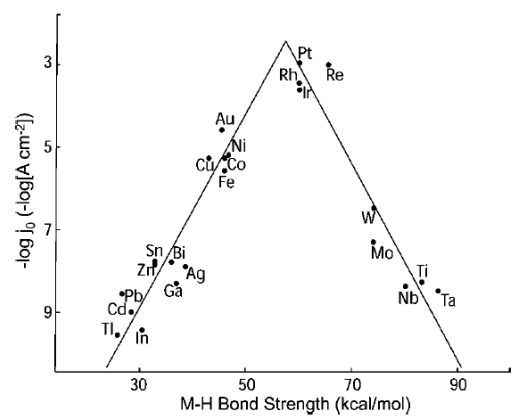

Figure 3.19: "Volcano plot", showing the exchange current density (which is an indicator for catalytic behaviour, see section 3.4.2) with respect to the hydrogen adsorption bond strength [13].

For the HER, the catalytic properties of a material seem to depends on the bond strength of protons with the surface of the metal[1], see figure 3.19.

[1]Also, a recent study by Quaino et al. on catalysts for the HER, especially the Volmer step, showed that the electronic band structure of the electrode is very important for catalyzing this reaction. Especially the location of the d-band with respect to the Fermi level of the metal seemed to be a key property. This also depends on the crystal structure of the surface. For more information, read [21].

3.4.2 Butler-Volmer equation

When a potential is applied to the electrode, the energy levels change. The level of the species in the bulk of solution, 'far' away from the electrode, remains the same (see figure 3.15 and also Appendix E), since the electrode does not influence it. However, the applied potential does change the energy level in the electrode and the height of the activation barrier with respect to both the oxidizing and reducing species [8][22]. This has been shown in figure 3.21.

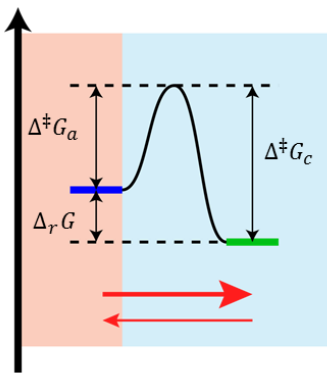

Figure 3.20: The activation energies for the anodic and cathodic reactions, $\Delta^{\ddagger}G_a$ and $\Delta^{\ddagger}G_c$ respectively. The total reaction energy is $\Delta_r G^{\ominus}$

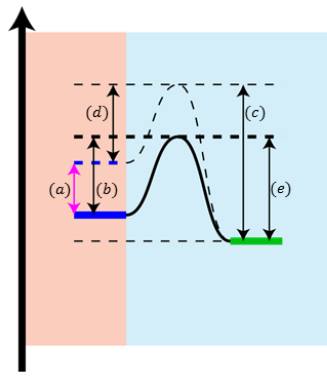

Figure 3.21: (c) and (d) represent the activation energies when no potential is applied. The activation energies change when a potential $\Delta\phi$ (a) is applied to (b) and (e)

The activation energy for the anodic ($\Delta^{\ddagger}G_a$) and cathodic($\Delta^{\ddagger}G_c$) process change when a potential is applied. They are not necessarily changed by the same amount. Depending on the properties of the transition state $\Delta^{\ddagger}G_a$ changes more than $\Delta^{\ddagger}G_c$ or the other way around[2]. The *cathodic transfer coefficient* α accounts for this potential inequality and has a value between 0 and 1. Experimentally however, the value usually turns out to be about 0.5 [8]. The activation energies $\Delta^{\ddagger}G_a$ and $\Delta^{\ddagger}G_c$ can be replaced by:

$$\begin{aligned} \Delta^{\ddagger}G_a &= \Delta^{\ddagger}G_a(0) - (1-\alpha)F\Delta\phi \\ \Delta^{\ddagger}G_c &= \Delta^{\ddagger}G_c(0) + \alpha F\Delta\phi \end{aligned} \tag{3.6}$$

where $\Delta^{\ddagger}G_a(0)$ and $\Delta^{\ddagger}G_c(0)$ are the activation energies without an applied potential for the anodic and cathodic processes respectively (see figure 3.21. With a small simplification:

$$f = \frac{F}{RT} \tag{3.7}$$

the anodic and cathodic current densities can now be described by:

$$\begin{aligned} j_a &= nFB_c[Ox]e^{-\Delta^{\ddagger}G_a(0)/RT}e^{(1-\alpha)nf\Delta\phi} \\ j_c &= nFB_a[Red]e^{-\Delta^{\ddagger}G_c(0)/RT}e^{-\alpha nf\Delta\phi} \end{aligned} \tag{3.8}$$

At the equilibrium potential $E^{\ominus}$, the reaction is in equilibrium (see figure 3.22), meaning that the anodic and cathodic processes take place at the same rate; j_a and j_c are equal [8]. The **exchange current density** j_0 has been defined as the value j_a or j_c when at $E^{\ominus}$:

[2]The transition state is the state in between the reactant and product state, on top of the activation barrier. For more information on this and the properties of the transition state, see [8]

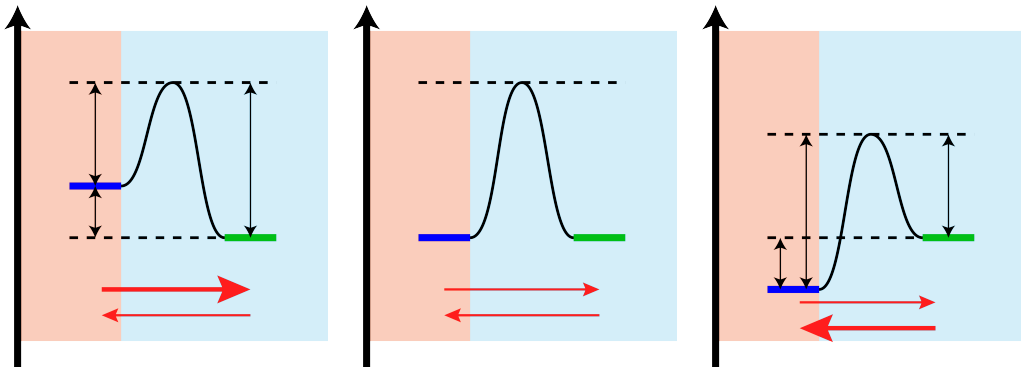

(a) Anodic flow (b) Equilibrium (c) Cathodic flow

Figure 3.22: Three different configurations of the energy levels. The double layer at the interface is kept out of consideration [17].

$$\begin{aligned} j_0 &= nFB_a[Red]e^{-\Delta^{\ddagger}G_a(0)/RT}e^{(1-\alpha)nfE^{\ominus}} = \\ &= FB_c[Ox]e^{-\Delta^{\ddagger}G_c(0)/RT}e^{-\alpha nfE^{\ominus}} \end{aligned} \tag{3.9}$$

The **overpotential** is defined as the difference between the electrode potential $\Delta\phi$ and the equilibrium potential of the reaction $E^{\ominus}$:

$$\eta = \Delta\phi - E^{\ominus}$$

Implementing Eqs. (3.9) and (3.4.2) leads to a simpler form of the Eqs. (3.8):

$$\begin{aligned} j_a &= j_0 e^{(1-\alpha)nf\eta} \\ j_c &= j_0 e^{-\alpha nf\eta} \end{aligned} \tag{3.10}$$

Using these simplified forms of the anodic and cathodic current densities, eq. (3.5) can be rewritten to:

$$j = j_0 \cdot \left\{ e^{1-\alpha)nf\eta} - e^{-\alpha nf\eta} \right\} \tag{3.11}$$

which is generally known as (a simplified form of) the **Butler-Volmer equation**. In figure 3.23 the behaviour of eq. (3.11) has been plotted. Such a plot is called a **Tafel plot**. See Appendix C for a more details about Tafel plots.

At the equilibrium potential $E^{\ominus}$, where η is equal to zero, the net current density j_0 goes to zero. At higher potentials, the current is anodic, while at lower potentials, the current is cathodic. For a metal like zinc, this means that at potentials higher than $-0.76V$, the metal will oxidize ($Zn(s) \rightarrow Zn^{2+} + 2e^-$), while below this value, zinc ions will reduce ($Zn^{2+} + 2e^- \rightarrow Zn(s)$), see figure (3.23)

Positive overpotentials occur for $j > 0$, which means there is an anodic current flowing. This corresponds to the upper branch, which will be called the **anodic branch** from now on. The lower branch, which corresponds to the cathodic current, will be called the **cathodic branch**, see figure 3.24.

A few things can be extracted from the Tafel plot:

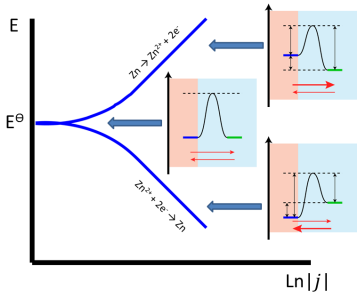

Figure 3.23: An illustrative Tafel plot of the Zinc-couple, together with the energy configurations of figure 3.22 [17].

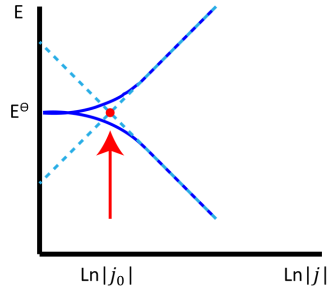

Figure 3.24: Simplifying a Tafel plot and determining the exchange current j_0.

1. If the high overpotential branches are extrapolated to $\eta = 0$V, $\ln|j| = \ln j_0$, see Appendix C. See the dashed line in figure 3.24 for an example.

2. α can be obtained from the slopes at high overpotential, see Appendix C.

3.4.3 Usage of Tafel Plots

Now that the overpotential η and exchange current j_0 have been explained, it has become possible to look at more than one electrode at a time. For example, for a situation of 2 electrodes, like in a galvanic cell, with the help of Tafel plots of both electrodes, one can:

1. explain the behaviour of an electrochemical cell or battery

2. show why it is important for a counter electrode to have a high exchange current j_0.

3. make it simpler to look for catalysts and improvement in catalytic behaviour (i.a. due to irradiation of light, in which we are interested, and as we will see later)

4. make the discussion of the results of the experiments 1 and 2 more intuitive, as will be seen in section 3.5.

If the two electrodes are connected by an electrical contact, the two electrodes are able to pass a current: one electrode accommodates the cathodic current, while the other does the this for the anodic current. Since there are only two electrodes:

$$I_{cathode} = -I_{anode} \tag{3.12}$$

and if the electrodes have the same surface area:

$$j_{cathode} = -j_{anode} \tag{3.13}$$

A potential can be applied between the two electrodes to achieve a few different situations:

1. $E_{app} = -E^0_{cell}$; in this case, both electrode potentials remain exactly at their equilibrium potentials, resulting in zero current. This corresponds to the left arrow in figure 3.25a.

2. $E_{app} = 0V$; here, the electrodes are connected and nothing else is done. The Fermi levels align, inducing overpotentials and a current starts to flow. This corresponds to the intersection of the two Tafel plots in figure 3.25a.

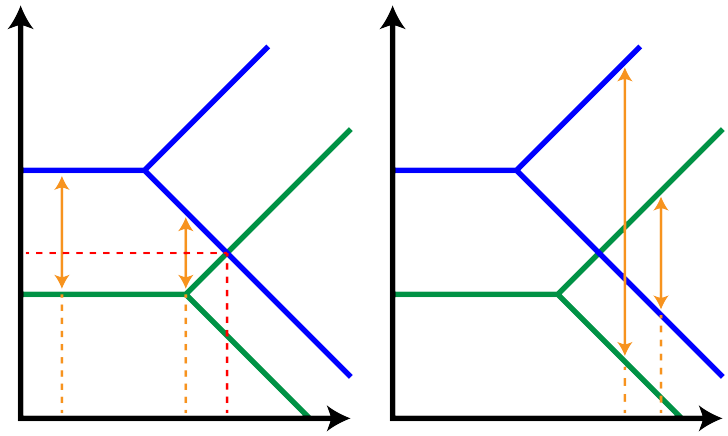

(a) Left arrow: no current flows in case of infinite resistance or opposing applied potential; right arrow: small resistance or small opposing applied potential; intersection: corrosion current and corrosion potential.

(b) Left arrow: reverse redox reaction with $E_{app} < -E^0_{cell}$; amplified redox reaction with $E_{app} > 0V$.

Figure 3.25: The different areas in the combined Tafel plots

3. $-E^0_{cell} < E_{app} < 0V$; in this region (right arrow in figure 3.25a), the applied potential slows down the redox reaction with respect to the reaction when it is allowed to run free, as in point 2. This is the most interesting region for the experiment discussed in section 3.3.

4. $E_{app} > 0V$; this means one provides larger overpotentials than the alignment of the Fermi energies provides: the redox reaction occurs at a faster rate. This situation corresponds to the right arrow in figure 3.25b.

5. $E_{app} < -E^0_{cell}$; this will result in the reverse redox reaction. This situation corresponds to the left arrow in figure 3.25b. This is important for water splitting cells.

The setup described in section 3.3 is a typical corrosion cell. The electrodes are both submerged in the same electrolyte, so in theory both the reduction and oxidation reactions can take place on just one electrode. If the right materials are used for both electrodes, the reactions take place mostly separately. This is what is done in corrosion engineering and protection. For Experiment 1 it does not really matter what kind of cell it is, as long as the NPG electrode passes a current. Still, to provide a foundation for this claim, the working principles of such a cell are described in Appendix D.

3.4.4 Hot Electron Injection in Adsorbate Electronic States

Hot electrons in silver and gold nanostructures have been shown to catalyse a number of chemical reactions. For example, plasmonic silver nanoparticles have catalytically driven oxidation reactions such as ethylene epoxidation, CO oxidation and NH_3 oxidation [23]. They have also been shown to assist in oxygen dissociation [23]. Another publication reports about hot electron-assisted dissociation of hydrogen gas into protons [24]. A review article by Linic et al. discusses a possible explanation of this hot electron behaviour [4].

A hot electron is injected into the electronic states of the adsorbate. Depending on the potential energy landscape, "the adsorbate can undergo a rapid reaction on the metal surface or it can move

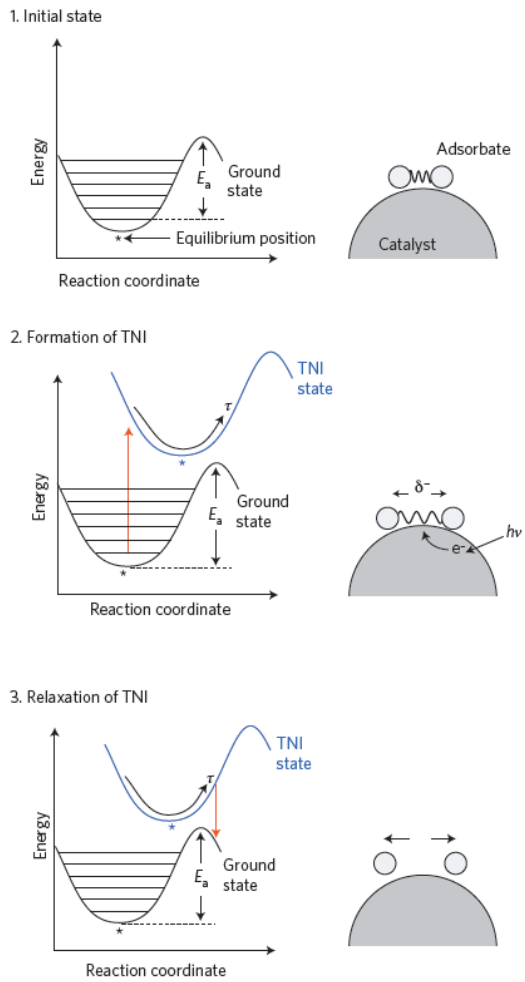

Figure 3.26: Mechanism of hot electron assisted adsorbate dissociation [4]. A hot electron enters the electronic states of the adsorbate which becomes a TNI state that decays after time τ. The adsorbate dissociates if the TNI decays on the other side of the activatin barrier of the ground state.

to the solution where it reacts" [4]. If the adsorbate undergoes the former of the two possibilities is usually called a transient negative ion (TNI). In this new TNI state, it is possible to move across the activation barrier of the 'ground state'. If the TNI state decays while it is located past this activation barrier, the reaction occurs [4]. Figure 3.26 is an illustration of this process. This is also how the mechanism is described in the publications about the hydrogen and oxygen dissociation [23][24].

Also, as hot electrons have more energy than 'cold electrons', they extend further away from the surface [24], see figure 3.27. If the hot electron meets an nearby electron acceptor, it can transfer into its electronic states [24], see figure 3.28.

3.4.5 Hydrogen Evolution Reaction in Detail and Rate Determining Step

The HER as previously discussed in section 3.2.3 is a simplification of the real process, which consists of more than one step. While the details of the reaction mechanisms are still largely unknown, the

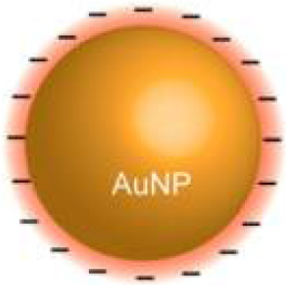

Figure 3.27: Since hot electrons have higher energy than the equilibrium Fermi distribution, they extend further from the surface of the particle [24].

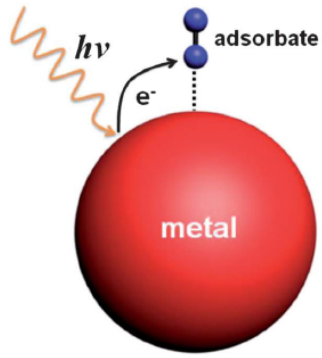

Figure 3.28: If an electron accepting species is near the surface of the particle, the extended hot electron can enter its electron states [25].

first step is believed to be [26][13][14]:

$$\mathrm{H}^+(aq) + e^- + s \rightleftharpoons \mathrm{H_{ad}} \tag{3.14}$$

A proton from solution adsorbs onto an active site s on the material and absorbs an electron. This reaction is known as the **Volmer reaction**. After this steps, one of two different steps is possible[26][13][14]:

$$\mathrm{H_{ad}} + \mathrm{H}^+(aq) + e^- \rightleftharpoons \mathrm{H_2}(g) + s \tag{3.15}$$

which is called the **Heyrovsky reaction**, and

$$\mathrm{H_{ad}} + \mathrm{H_{ad}} \rightleftharpoons \mathrm{H_2}(g) + 2s \tag{3.16}$$

which is the so-called **Tafel reaction**.

The HER on a normal gold electrode is believed to go through the first and second step [14]. However, as the activation energy depends strongly on the surface of the electrode, the focus in this report should not be biased towards only this path. And since the activation energies depend on the surface, also the**rate determining step** is not set.

The activation energy of a reaction also depend on the surface at which it takes place. Therefore, the **rate determining step** is not set. For a non-porous gold electrode, it is believed that the Volmer-reaction is the rate determining step (RDS), while this could be very different on a nanostructured surface.

Which reaction is the RDS can be deduced from the energy diagram of the reaction. The reaction with the highest transition state (which usually also means it has the highest activation energy) in general is the RDS [8].

3.5 Proposed Mechanism

Now suppose not the first, but the second step is rate-determining in the case of this experiment, see figure 3.29. And suppose the reaction for one species of reactant looks like this [8]:

$$v = k \cdot [R] \tag{3.1}$$

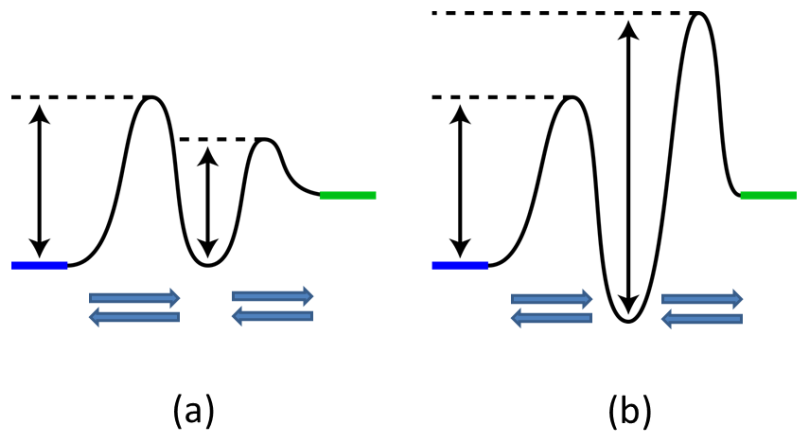

Figure 3.29: Activation barriers for a two-step reaction; (a) the first step is the RDS and the slowest step; (b) the seconds step is the RDS and the slowest step [8].

where v is the reaction rate, k the rate constant and $[R]$ the concentration of reactant. The reaction rates between state A (the reactant state), B (the intermediate state) and C (the product state) are

$$A \underset{k_2}{\overset{k_1}{\rightleftharpoons}} B \underset{k_4}{\overset{k_3}{\rightleftharpoons}} C \tag{3.2}$$

As C is the volatile H_2-gas, the concentration of $[C]$ is very low. Also assume that the concentration of A is constant, as A is replenished by the bulk of electrolyte. Then:

$$v_1 = k_1[A] = cst \tag{3.3}$$

The current flowing through the electrode is proportional to the rate of the RDS. See also eqs. (3.2) and (3.1). If this is the reaction from B to C,

$$j \propto k_3[B] - k_4[C] \simeq k_3[B] \tag{3.4}$$

Assume the activation energy of all the steps remains the same, so all the ks are constant. Then

$$j \propto [B] \tag{3.5}$$

To determine the concentration at which $[B]$ remains constant (i.e. all flows have become constant and system is at mass transfer equilibrium), one looks at the change of $[B]$, which depends on $[B]$ itself. $[B]$ increases with a constant amount v_1 and is decreased by two rates: v_2 and v_3:

$$\frac{d}{dt}[B](t) = v_1 - k_2[B](t) - k_3[B](t) = k_1 - (k_2 + k_3)[B](t) \tag{3.6}$$

This is a differential equation with the general solution:

$$[B](t) = \frac{v_1}{k_2 + k_3} + C_1 \cdot e^{-(k_2+k_3)t} \tag{3.7}$$

As k_2 and k_3 are assumed to be constant, this can be simplified to:

$$[B](t) = \frac{v_1}{K} + C_1 \cdot e^{-Kt} \tag{3.8}$$

with:

$$K = k_2 + k_3 \tag{3.9}$$

The equilibrium value of $[B]$ is found for $t \to \infty$:

$$[B]_{eq} = \frac{v_1}{K} \tag{3.10}$$

At $t = 0$:

$$C_1 = [B]_{t=0} - [B]_{eq} \tag{3.11}$$

In the case that illumination of the NPG would lead to an increased reaction rate for the first step due to hot electron injection or a plasmon related mechanism, the v_1 would change:

$$v_1' = k_1[A] + v_{ph} \tag{3.12}$$

If the amount of generated hot electrons is proportional to the intensity of the light (as is suggested in [24] and [23]:

$$v_{ph} = k_{ph}(\lambda) \cdot I(\lambda) \tag{3.13}$$

where k_{ph} is a factor that can written as a product two separate parts:

$$k_{ph} = \beta_0(\lambda) \cdot e^{-\Delta^{\ddagger} G_a} \tag{3.14}$$

Here, β_0 is a parameter that contains information about the conversion efficiency of photons to reaction events of the nanoporous metal. It depends on the nanostructure of the metal, the wavelength the light, the dielectric medium in the pores, λ (see chapter 2), the efficiency with which the plasmons increase the reaction rate and probably more variables. If everything in the system remains the same and only the light intensity is variable, β_0 would be a constant. The second component of eq. (3.14) is again the influence of the activation barrier, see eq. (3.3).

It could be, for example, that hot electrons participate in the Volmer reaction (see section 3.4.5) and not the other steps. As explained in section 3.4.1, hot electrons have an extended reach from the surface of the metal. It is possible that such an electron would enter the electronic levels of a proton to make it adsorb onto the surface of the metal. Looking at eq. (3.14), it could be that the hot electron provides a reaction site s together with an electron e^- for this reaction. If this is true, it might explain why a photovoltage is measured (see section 3.3.2). If actually the second step of the HER (Tafel or Heyrovsky) is the step that the equilibrium potential belongs to, increasing the concentration of B would also change the equilibrium potential. This would result in a different cell potential. This has also been stated in section 3.3.2.

So, if before $t = 0$ the dark system is passing current and at mass transfer equilibrium ($[B]_{t \leq 0} = [B]_{eq}$) and at $t = 0$ the light is turned on, the $[B]$ after $t = 0$ would be

$$[B](t, t > 0) = [B]_{eq}' - \frac{v_{ph}}{K} \cdot e^{-Kt} \tag{3.15}$$

with

$$[B]_{eq}' = \frac{v_1'}{K} = \frac{k_1[A] + v_{ph}}{K} \tag{3.16}$$

From now on, $[B](t, t > 0)$ will be denoted as $[B](t)$ where $t = 0$ is the moment on which the light is turned on.

Eq. (3.15) can be rewritten into a more intuitive form by using eq. (3.16):

$$[B](t) = [B]_{dark} + [B]_{light} = [B]_{dark} + \frac{v_{ph}}{K} \cdot (1 - e^{-Kt}) \tag{3.17}$$

Following from eq.(3.5), the current is proportional to $[B]$:

$$j \propto [B]_{dark} + \frac{v_{ph}}{K} \cdot (1 - e^{-Kt}) \tag{3.18}$$

Therefore, the following holds for the time-dependent photocurrent:

$$j_{ph} \propto \frac{v_{ph}}{K} \cdot (1 - e^{-Kt}) \tag{3.19}$$

At $t \to \infty$, together with eqs. (3.13) and (3.14), and if k_2 and k_3 are constant (as was assumed earlier), this would become:

$$j_{ph} \propto \beta_0(\lambda) \cdot I(\lambda) \cdot e^{-\Delta^{\ddagger} G_a} \tag{3.20}$$

From this final proportionality of the photocurrent, a few things can be concluded:

- The photocurrent would increase of the intensity $I(\lambda)$ of the light is increased. This is in agreement with [23] and [24] and expectations. This has not been tested during the experiments of this project however.
- The photocurrent would depend on the wavelength λ of the light. If hot electrons or plasmons are driving the reaction, the conversion efficiency of photons to plasmons and hot electrons depends on the resonance frequency of the nanoporous metal. This, in turn, depends on the geometrical properties of the nanostructure (see Ch. 2), the metal itself, the surrounding medium (see Ch. 2 and [27]). These properties are all contained in β_0.
- Also, the photocurrent would depend on the activation barrier height of the reaction step that is influenced by the hot electrons. It could be that the height of this barrier depends on the electric field at the surface. This might be an explanation of photocurrent only being observed when the two electrodes were near each other, see section 3.3.2.

Such a mechanism could also be true for a different reaction. For example, in neutral systems (with pH=7), there would be a lot of water molecules on the surface of the metal. Hot electrons could assist in dissociation of the water just as it does for oxygen and hydrogen gas (see section 3.4.4). This dissociation of water is also the mechanism of hydrogen production in alkaline electrolytes [6]:

$$\mathrm{H_2O}(l) + e^- + s \leftrightharpoons \mathrm{H_{ad}} + \mathrm{OH^-}(aq) \tag{3.21}$$

3.6 Conclusion

Plasmonic nanoparticles can be used to improve semiconductor photovoltaic cells and enhance hydrogen production by semicondutor water splitting cells. In order to determine whether nanoporous metals have similar properties as the nanoparticles, an experiment has been performed using a plain NPG electrode in a corrosion cell. A photovoltage and photocurrent were measured, but their behaviour was not as it was expected as it took a long time (order of 10 to 100s of seconds) for the . A possible mechanism has been proposed that would explain this behaviour which takes into account the different reaction steps in the HER. However, to make solid conclusions about the photoactive mechanism and the exact extent of the photo-enhancement, more experiments should be performed in a better understood environment, as this is a very complex system. Also, more theory should be investigated. See section 3.7 for recommendations about future experiments and future work to be done on this subject.

3.7 Recommendations

3.7.1 On NPG

To better investigate the photo-enhancing properties of NPG, more experiments have to be done. To determine whether the enhancement is really due to plasmonic activity, one should do experiments with monochromatic light of different wavelengths. If the process is plasmonic, the largest photoeffect will be measured at the localized surafce plasmon resonance wavelength of the nanoporoous gold. Also, one should vary the intensity in these experiments to check whether the proposed mechanism in section 3.5 could be true or not.

And apart from proving that the concept works, it is of course important to compare the efficiency of the new device with other devices, to see if there already is an indication that this new device might become competitive on the market with all the other types of devices. For good comparison and for reducing the complexity of the system, in new experiments a few things have to be applied:

- Measurements should be done using a three-electrode setup. This method removes the contribution of the counter electrode to the measured cell potential, which makes the characteristics of the NPG electrode better researchable.
- Measurements should be performed at constant potentials, to remove any time-dependent artefacts from the measurements, such as electric double layer charging or concentration equilibration.
- Ion transport should be made more easy, by, for example, having the electrode in direct contact with the bulk electrolyte, instead of using a filter paper to transport electrolyte. This way the concentration of ions at the surface is better to control and more likely to have similar concentrations as the bulk of the electrolyte.
- Work at standard conditions or known constant conditions. This way the cell potential is less sensitive to concentration changes and the results are better comparable with other studies.

If these experiments are done, more things can be said about the NPG electrode. Since most of the environment is constant in this way, it is easier to determine what contributes to the photo-enhancement and what does not.

Also, in section 3.3.2 it has been observed that the distance between the two electrodes is important to the photo-effect. This could be linked to the electric field between them. Such a field might have influence on the electric double layer or the activation barrier. It is even likely that the two are linked. This should be further investigated, experimentally and theoretically.

To assist with the investigation of the surface reactions, one could look at the Tafel slope. This could provide some details about the rate determining step in the reaction. For more information, read [13][14].

But even though the HER is one of the most investigated chemical reactions, the details of the reaction steps are still largely unknow [13][14]. Since the reaction is so strongly dependent on the surface, the details of the reaction on an NPG surface are even less likely to have been discovered.

3.7.2 Other Materials and Other Processes

Gold, of course, is expensive. Producing devices based on NPG on large scale is not likely to be realised in the future due to the costs. However, using the same principle, namely that of generation localized surface plasmon resonance and hot electrons on nanoporous metals, one could look for other metals or alloys that have comparable properties, but are a lot cheaper to use. One could look at the so-called Volcano plot, in which one can see a number of materials that are catalysts for the HER or not. To look for the best material for photo-catalysis, one needs to find a metal that

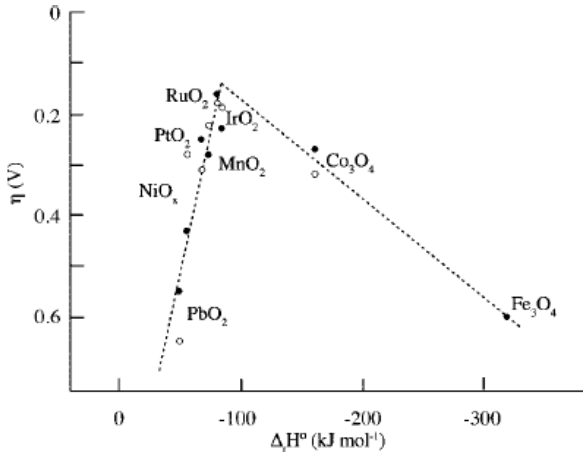

Figure 3.30: Volcano plot of OER catalysts [13]. Mostly consists of (metal) oxides. Closed circles: in acid. Open circles: in alkaline media.

hardly corrodes, that has good catalytic properties already, that is cheaper than gold (since it is still supposed to be used in devices) and that has a plasmon resonance frequency in the visible range of the electromagnetic spectrum.

Apart from the HER, also the OER is of interest. In general a few HER catalysts are known that hardly require any overpotential. For the OER, this is different. Metals require a large overpotential to drive the OER. Metal oxides do a better job (see figure [BLAAT Volcano for OER]). Creating a plasmonic metal with an oxide layer that catalyses the OER could be a huge improvement in water splitting cells.

Also, as this report shows, metals can photo-catalyse a reaction, but they have not been shown to harvest energy from light. In order to make a device that does not need any other energy input other than light, one needs charge separation. A metal cannot do charge separation. Combining it with a semiconductor therefore looks like a required step to achieve such a device.

References

[1] J. Lee, S. Mubeen, X. Ji, et al. "Plasmonic Photoanodes for Solar Water Splitting with Visible Light". In: *Nano Lett.* (2012).

[2] C.Y. Chiang, K. Aroh, et al. "Copper Oxide Nanoparticle Made by Flame Spray Pyrolysis for Photoelectrochemical Water Splitting -Part II. Photoelectrochemical Study". In: *Internation Journal of Hydrogen Energy* (2011).

[3] S.Y. Reece et al. "Wireless SOlar Water Splitting Using Silicon-Based Semiconductors and Earth-Abundant Catalysts". In: *Science* (2011).

[4] S. Linic, P Christopher, and D.B. Ingram. "Plasmonic-metal nanostructures for efficient conversion of solar to chemical energy". In: *Nature Materials* (2011).

[5] L. de Jeer. "Light Induced Hydrogen Evolution on Nanoporous Gold Film". MA thesis. University of Groningen, 2013.

[6] M. Grätzel. "Solar Cells to Dye For". In: *Nature* (2003).

[7] M. Grätzel. "Photoelectrochemical Cells". In: *Nature* (2001).

[8] *Physical Chemistry.* Oxford University Press, 2006.

[9] *Principles of Corrosion Engineering and Corrosion Control.* Elsevier, 2006.

[10] P. Vanýsek. *ElectrochemicalSeries*.

[11] *Corrosion Engineering: Principles and Practice*. McGraw-Hill, 2008.

[12] R.C. Kainthla and J. O'M. Bockris. "The Redox Potential and the Fermi level in Solution". In: *J. Phys. Chem.* (1987).

[13] M.G. Walter, E.L. Warren, J.R. McKone, et al. "Solar Water Splitting Cells". In: *Chem. Rev.* (2012).

[14] Z. Tang, L. Liao, et al. "Temperature Effect on Hydrogen Evolution Reaction at Au Electrode". In: *Chin. J. Chem. Phys.* (2012).

[15] A. Trügler. "Optical Properties Of Metallic Nanoparticles". PhD thesis. University of Graz, 2011.

[16] O. Neumann, A.S. Urban, et al. "Solar Vapor Generation Enabled by Nanoparicles". In: *ACS Nano* (2013).

[17] D. Diesing, G. Kritzler, et al. "Metal/Insulator/Metal Junctions fo Electrochemical Surface Science". In: *Journal of Solid State Electrochemistry* (2003).

[18] M. Bangsubcharoen. "A Study of Triboelectrification for Coal, Quartz and Pyrite". PhD thesis. Virginia Polytechnic Institute and State University, 1999.

[19] J.E. Guyer, W.J. Boettinger, et al. "Model of Electrochemical "Double Layer" Using the Phase Field Method". In: *Physica D* (2002).

[20] *Fuel Cells: From Fundamentals to Applications*. Springer, 2006.

[21] P. Quaino, E. Santos, et al. "Recent Progress in Hydrogen Electrocatalysis". In: *Advances in Physical Chemistry* (2011).

[22] *High Energy Density Lithium Batteries*. Wiley, 2010.

[23] P. Christopher, H. Xin, and S. Linic. "Visible-light-enhanced catalytic oxidation reactions on plasmonic silver nanostructures". In: *Nature Chemistry* (2011).

[24] S. Mukjherjee, F Libisch, .N Large, et al. "Hot Electrons Do the Impossible: Plasmon-Induced Dissociation of H_2 on Au". In: *Nano Lett.* (2012).

[25] M. Xiao, R. Jiang, F. Wang, et al. "Plasmon-Enhanced Chemical Reactions". In: *Journal of Materials Chemistry A* (2013).

[26] E. Skúlason, G.S. Karlberg, J. Rossmeisl, et al. "Density functional theory calculations for the hydrogen evolution reaction in an electrochemical doulb elayer on the PT(111) electrode". In: *Phys. Chem. Chem. Phys.* (2007).

[27] X. Lang, P. Guan, et al. "Localized Surface Plasmon Resonance of Nanoporous Gold". In: *Applied Physics Letters* (2011).

[28] *Materials Degradation and Its Control by Surface Engineering*. Imperial College Press, 2011.

General Conclusion

In this report, two projects have been discussed.

During the first project, nanoporous gold (NPG) was synthesized and the ligament and pore sizes were tailed by chemical coarsening. For different feature sizes, the transmission peak was measured. An attempt was made to correlate ligament diameter, pore diameter and their ratio with the peak wavelength. However, no clear correlation was found. After investigating the Bruggeman Effective Medium theory, it was discovered one might have to look at a correlation between the aspect ratio and the peak wavelength. A first exploration of this correlation showed promising results.

The second project consisted of providing a theoretical support for the experimental works of De Jeer (Master thesis) and Detsi (Postdoctoral project). An experiment was performed with NPG to determine whether it had the same plasmonic and photocatalytic properties as plasmonic nanoparticles. However, the results were different than expected, with a slow time-component. A mechanism has been proposed to try to explain this time-component. The mechanism deals with the multiple steps of the hydrogen evolution reaction, rate determining steps and hot electrons. A few experiments can and have to be performed to determine whether this mechanism is a description that is close to reality. One of the conclusions of this project is that the system that has been investigated is very complex and a few measures have been proposed to make it less complex and the influences of different variables better distinguishable.

What can be concluded from both projects, is that nanoporous gold is indeed photoactive and its resonance peak can be tuned by tuning the features of the microstructure. Also, after investigating publications on plasmonic water splitting, it was concluded that the combination of a plasmonic metal with a semiconductor seems to be the best way to take advantage of the plasmonic properties. Overall, NPG is a promising new material for solar water splitting and other light-harvesting and photoactive devices

Acknowledgements

First of all, I would to thank dr. Eric Detsi for being my daily supervisor for the past one and a half year. He showed me how thrilling it is to be involved in research and to be able to follow up on any interesting lead. He allowed me to work on my own and taking my own directions while staying involved in my work. And he has done many experiments and theoretical work that benefited my project. The inexhaustible enthusiasm with which he does research motivated and inspired me enormously.

I would also like to thank prof. De Hosson for allowing me to work in his group. The two projects have been very enjoyable and I learned a lot in the time that I have been working here. And I would like to thank Leo de Jeer for doing the experiments, thinking along with the theoretical work I did and letting me be part of his Master project. And of course I would like to thank the entire Materials Science group for assisting me with equipment, machines and software and for providing a friendly environment and atmosphere.

Appendix C

Tafel Plots

In both the anodic and cathodic current densities of the Butler-Volmer equation (eq. (3.11)), it becomes clear that there are two regions in which the current density behaves differently: the region with low overpotential and the region with high overpotential. This can also be observed in figure 3.23.

At low overpotential ($\eta < 0.01V$)[8] eq. (3.11) can be approximated by:

$$j = j_0 n f \eta \tag{C.1}$$

using the expansion of e^x:

$$e^x = 1 + x + ... \tag{C.2}$$

Eq. (C.1) shows that, for low overpotentials, the current density is proportional to the overpotential: in this region the interface behaves like an Ohmic contact. For large positive overpotentials ($\eta > 0.12V$), the second term of Eq. (3.11) becomes much smaller than the first term, so the second term can be neglected [8], resulting in:

$$j = j_0 \, e^{(1-\alpha)nf\eta} \tag{C.3}$$

For large negative overpotentials ($\eta < -0.12V$), the same can be said, only for neglecting the first term:

$$j = -j_0 \, e^{-\alpha n f \eta} \tag{C.4}$$

A different but useful way to display the Tafel diagram is by plotting the overpotential η (or the electrode potential) versus $\ln|j|$, since, from Eqs. (C.3) and (C.4):

$$\ln|j| = \begin{cases} \ln j_0 + (1-\alpha)nf\eta & \text{for } j > 0 \\ \ln j_0 - \alpha n f \eta & \text{for } j < 0 \end{cases} \tag{C.5}$$

Since n and f are usually known and η can be measured or accurately applied, the transfer coefficient α can be obtained from the slope of the plot at high overpotentials. Also, the exchange current can be obtained by extrapolating the slope at high overpotential to the region with low overpotential, as shown in figure 3.24.

This can also be used to write the overpotential as a function of current density:

Appendix D

Corrosion

If a metal like zinc is submerged into a solution of acid, a redox reaction will occur: the zinc will dissolve and hydrogen will be produced. This can be concluded from table D.1 together with eqs. (3.9) and (3.11).

Redox couple	Reduction potential (V) vs. SHE
$Zn^{2+} + 2e^- \rightleftharpoons \mathbf{Zn}(s)$	-0.76
$Pt^{2+} + 2e^- \rightleftharpoons \mathbf{Pt}(s)$	$+1.18$
$2\mathbf{H}^+ + 2e^- \rightleftharpoons H_2(g)$	0.00

Table D.1: Redox couples zinc, platinum and hydrogen with their reduction potentials. The available elements of the example are shown boldfaced.

If the zinc is in electrical contact with another metal, platinum for example, it is experimentally observed that the hydrogen reaction (HER) mainly takes place on the platinum electrode instead of the zinc electrode [9]. This can be explained by looking at the exchange currents of the HER on the two metals. As explained in section 3.4.1 the exchange current j_0 is high when the activation energy is low, i.e. when the material is a catalyst for the specific reaction. Platinum is a catalyst for the HER with a high exchange current, while zinc is not, see table D.2.

Electrode	Redox couple	exchange current $A\,cm^{-2}$
Zn	$Zn^{2+} + 2e^- \rightleftharpoons Zn(s)$	$\sim 10^{-3}$
	$2H^+ + 2e^- \rightleftharpoons H_2(g)$	$\sim 10^{-10}$
Pt	$2H^+ + 2e^- \rightleftharpoons H_2(g)$	$\sim 10^{-3}$

Table D.2: The redox couples of table D.1 with their exchange currents j_0 at a platinum and a zinc electrode [28].

From section 3.4.1 we know that the Fermi energies of two metals in electrical contact are equal. Therefore, the overpotential for the HER is the same on both electrodes, but because the exchange currents are different, the catalyst allows for a much higher current. This is shown in figure D.1. From this figure it can be deduced that the HER is strong on the platinum electrode, while weak on the zinc electrode. Also, the zinc electrode dissolves more rapid compared to the case in which there was no platinum, which would be the intersection of the dark blue and green lines [9].

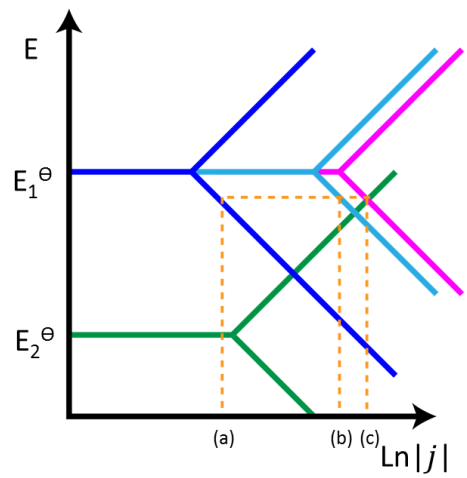

Figure D.1: Combined Tafel plot of the Al/Al^{3+} couple (green) and the $H_2/\ 2H^+$ couple on Al (dark blue) and Au (light blue). The purple line represents the sum of the two blue lines. At the intersection of the green and purple line, the current and potential are called the corrosion current j_{corr} (c) and the corrosion potential E_{corr} respectively. All electrodes are at the same potential at this point, which means that the cathodic currents through the platinum and aluminium electrode can be found by looking at the same potential. It can be seen that the current through the aluminium electrode (a) is very small, while the current through the platinum electrode is high (b) [9].

With this, one can also explain why the cell potential of the cell in the experiment (section 3.3) is not equal to the calculated cell potential. If one would put a voltmeter between the two electrodes, no current flows from the one to the other electrode. However, the redox reaction between hydrogen and aluminium does not need an extra electrode: it is only improved by another electrode. While the aluminium is oxidizing, the electrode has an overpotential (as it is passing a current).

This can also be seen in figure D.1. When the two electrodes are in electrical contact, the intersection of the purple line and the green line will represent the situation. However, when the platinum electrode is disconnected or a voltmeter is between it and the aluminium, the light blue curve will not pass any current: the electrode would 'be' on the curve at very low j. The HER on aluminium is still allowed to occur, so the intersection of the dark blue and the green line is represents this situation. The aluminium will have an overpotential. The potential at the intersection is called the corrosion potential E_{corr}. The difference between the platinum electrode and the aluminium electrode becomes:

$$E^0_{cell} = E_{red} - E_{corr} < E_{red} - E_{ox} \quad (= 1.66V \text{for this experiment}) \tag{D.1}$$

Appendix E

Concentration Overpotential

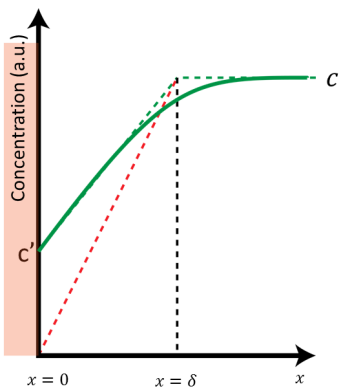

Figure E.1: Nernst layer with a thickness δ. Far away, the bulk concentration is constant (c), while the concentration at the surface c' depends on the reaction rate and the diffusion speed D. The dashed line approximates the concentration profile for c'=0 [8].

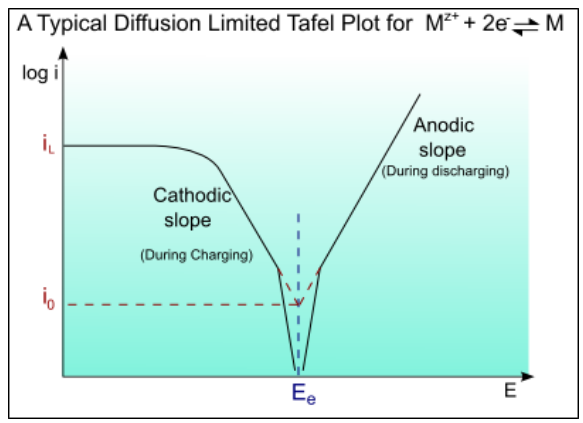

Figure E.2: Tafel plot where the cathodic branch is diffusion-limited. Image from www.doitpoms.ac.uk/tlplib/batteries/ printall.php

As the HER or any other reaction takes place at the surface of an electrode, the concentration of reactant decreases. This is compensated by a flow of reactant from the bulk of the electrolyte. However, if the reaction rate is very high, the diffusion is too slow and the reactant concentration at the surface is very different from that in the bulk electrolyte. The zone in which the concentration of reactant is in between the bulk concentration and the surface concentration is called the *Nernst diffusion layer*, see figure E.1. If the reaction is so fast that the concentration at the surface becomes zero, the current cannot become higher: there just is not enough reactant at the surface to donate or accept more electrons. The current at which this happens is called the limiting current j_{lim}[8]:

$$i_{lim} = \frac{nFD}{\delta}c \tag{E.1}$$

As seen in section **??**, the current depends on the concentration at the surface. At a certain electrode potential, if the concentration is low, the current is low too, due to the concentration

factor in eqs. (3.2) and (3.1). And if the concentration is high, the current is high. So if the concentration at the surface is lower than it could be, the current is lower than it could be, for this electrode potential. Therefore this can be seen as another overpotential, called the *concentration, polarization or mass-transfer overpotential*[8]:

$$\eta^c = \frac{RT}{nF} \ln\left(1 - \frac{j\delta}{ncFD}\right) \tag{E.2}$$

Appendix F

Background Cell Potential

The (time-dependent) shape of the dark part of V_{oc} (see figure 3.8) can be explained as follows.

Q from eq. (3.4) for the redox reaction of Experiment 1 (eq. (3.1)) is

$$Q = \frac{a_{Al}^2 \cdot a_{H+}^6}{a_{Al^{3+}}^2 \cdot a_{H_2}^3} \tag{F.1}$$

The activity of a solid is equal to 1 [8] and the approximation is made that the activity of hydrogen gas is equal to its fugacity p_{H_2} [8]. In equilibrium, the ionic activities are equal to their concentrations [8]. This turns eq. (F.1) into

$$Q = \frac{[H^+]^6}{[Al^{3+}]^2 \cdot p_{H_2}^3} \tag{F.2}$$

Since there is no hydrogen bubbled through the solution and there is no concentration of aluminium ions in the electrolyte at $t = 0$, it is difficult to calculate this Q. Therefore, it is only used to explain the behaviour of the voltage in the plot.

At zero-current, the concentrations at the surface of the electrodes are equal to the concentrations in the bulk of the electrolyte. The reaction quotient for this case is called Q^0. For a working cell, the concentrations at the surface change as reactants are being used by the reaction and products are formed (see also Appendix E). Protons are reduced into hydrogen gas, so H^+ decreases and p_{H_2}

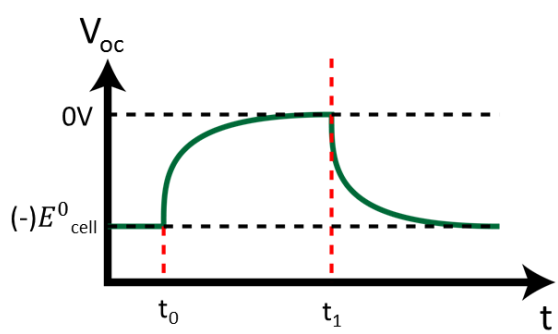

Figure F.1: The background voltage. At t_0 electrical contact is established. At t_1 the current is blocked and the concentrations go back to their values of before t_0

[PLAATJE MOET NOG FF VERANDEREN (gaat direct naar 0V)].

increases. Also, $[Al^{3+}]$ increases, since there was none before and the electrolyte does not contain any aluminium ions yet. However, after a certain time t, the concentrations and fugacity become constant when the reaction rate and diffusion rate balance each other out (see the flat region just before t_1 in figure F.1). The reaction quotient related to this state is Q_1. It consists of all of the activities at this point, which can not be assumed to be equal to the concentrations any longer [8][9]. This is no problem, because the concentrations do serve as an indication of Q_1 with respect to Q^0. Since $[H^+]$ has decreased and $[Al^{3+}]$ and p_{H_2} have increased,

$$Q_1 > Q^0$$

which also means that, from eq. (3.6):

$$E'_{cell} < E^0_{cell} \tag{F.3}$$

The cell potential E^0_{cell} is 0V at the constant reaction quotient Q_1, since the electrodes are in electrical contact. As soon the contact is removed (i.e. the multimeter is switched to voltmeter), the current stops flowing immediately and with it the concentrations at the surface start to get back to their original values of Q^0. The voltmeter shows a voltage going from 0V to E^0_{cell} in a smooth inverse exponential as diffusion decreases when Q approaches Q^0. This has been shown in figure F.1 after t_1.

Appendix G

Three Electrode Voltammetry Experiment

G.1 Three Electrode Voltammetry

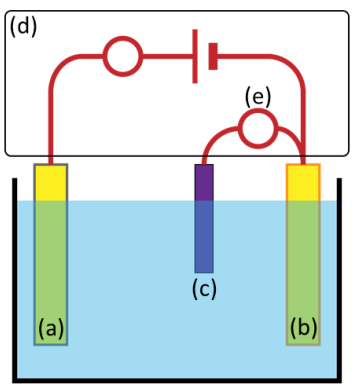

Figure G.1: Schematic representation of a three-electrode setup. (a)Counter electrode; (b) Working electrode; (c) Reference electrode; (d) Potentiostat controlling the potential of (b) with respect to (c) and making sure (a) delivers enough current. The voltmeter (e) measures the difference between (b) and (c) and prevents any current from flowing though the reference electrode.

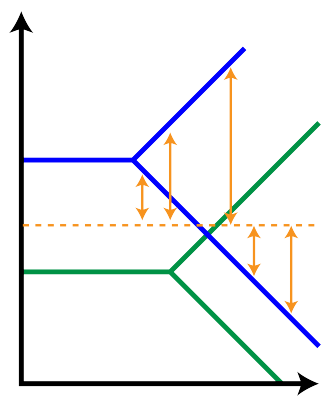

Figure G.2: Tafel plot for three-electrode setup. The dashed orange line represents the constant potential of the reference electrode. The potential of the working electrode is measured (and controlled) with respect to this potential. In this case, the blue reaction is the one taking place at the working electrode.

A schematic of a three-electrode setup is shown in figure G.1. The potential difference is measured between the reference electrode and the working electrode:

$$E_{measured} = E_{working} - E_{reference} \tag{G.1}$$

while the counter electrode serves only as a source or sink of electrons. The benefit of this method is that the reference electrode does not pass any current. This means that nothing happens with the concentrations of ions around the reference electrode. This results in the ability to use eq. (G.1)

to measure the electrode potential of an electrode relative to this constant potential. With a device called a **potentiostat**(see figure G.1) a potential difference can be applied and maintained between the working electrode and the reference electrode, while the current through the working electrode is measured, providing the data for a Tafel plot (see figure G.2).

G.2 Experiment: NPG and Three-electrode Voltammetry

The idea of this experiment was to take a closer look at the NPG electrode on its own. The previous experiment was a two-electrode experiment, which is difficult to control, since both electrodes are effected when something is changed. A three-electrode system takes this difficulty away. As explained in Appendix G, the potential of the working electrode is tuned with respect to a constant reference electrode.

G.2.1 Methods and Materials

The setup of the experiment consisted of an NPG working electrode, a saturated calomel electrode as reference electrode, water of pH=7 as electrolyte and a potentiostat to control the potentials and currents and measure them. As counter electrode, a gold or platinum electrode is used. Linear sweep voltammetry is performed to with and without light to see the photo-enhancement. Also, the dark and photocurrents were measured at a few fixed potentials.

G.2.2 Results

Figure G.3 shows the results of the linear sweep voltammetry and the fixed potential measurements. It is clear that there is a photo-enhancement. However, what is also clear, is that the two methods do not yield the same results, even though they measure at the same potentials. To be sure there are no dynamic effects like a long equilibration time, it is best to measure the current at fixed potentials. This is also how in general Tafel plot data are obtained. However, to observe a photo-enhancement, the linear sweep is sufficient.

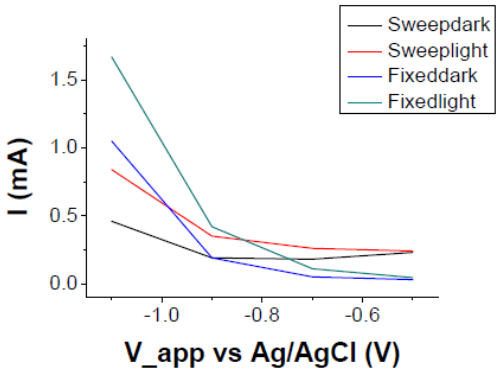

Figure G.3: Current for dark and light case, measured by potential sweep and at fixed potentials [5]. It can be seen that, although the system is the same, the results depend on the measurement method.

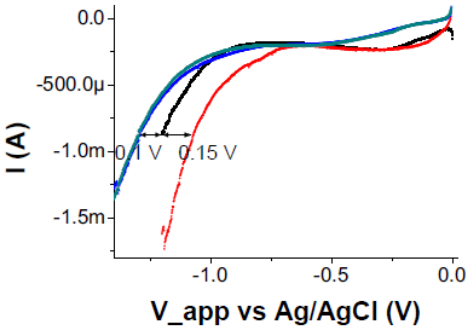

Figure G.4: Detailed potential sweep of HER on NPG in pH=7 water as electrolyte [5].

A more detailed sweep of the HER on NPG is shown in figure G.4. A solid gold electrode has been compared with the NPG electrode for the dark and illuminated situation. As can be observed, the solid gold electrode has no photoresponse, while the NPG has. Also, the NPG passes more current than the solid gold electrode in the dark. This can be attributed to the larger surface area of NPG with respect to solid gold electrode. More surface means more current.

G.3 Conclusion

The conclusion of this experiment/appendix should be that there is indeed photoactivity on the NPG. The experiment should be performed again, but with the changes mentioned in the Recommendations section of the report (section 3.7).